École des Ponts ParisTech

Novosibirsk State University

*THE REAL SCIENCE

Research Internship

Field of Study: GMM

Scholar Year: 2018-2019

The study of coherent structures based on numerical algorithms of nonlinear Fourier transform for a nonlinear Schrödinger equation

Confidentiality Notice

Non-confidential report

Author:

Egor Sedov — Génie Mécanique et Matériaux

Promotion:

2019

ENPC ParisTech Tutor:

Alain Maruani

Host Organism Tutor:

Sergei Turitsyn

Internship from 01/02/2019 to 31/08/2019

Name of the host organism: École des Ponts ParisTech

Address: 2 rue Pirogova

630090 Novosibirsk

Russia

Confidentiality Notice

This present document is not confidential. It can be communicated outside in paper format or distributed in electronic format.

Abstract

The nonlinear Schrödinger equation (NLSE) is often used as a master path-average model for fiber-optic links to analyse fundamental properties of such nonlinear communication channels. Transmission of signal in nonlinear channels is conceptually different from linear communications. We use here the NLSE channel model to explain and illustrate some new unusual features introduced by nonlinearity. In general, NLSE describes the co-existence of dispersive (continuous) waves and localised (here in time) waves — soliton pulses. The nonlinear Fourier transform method allows one to compute for any given temporal signal the so-called nonlinear spectrum, that defines both continuous spectrum (analogue to conventional Fourier spectral presentation) and solitonic components. Nonlinear spectrum re- mains invariant during signal evolution in the NLSE channel. We examine conventional orthogonal frequency-division multiplexing (OFDM) and wavelength-division multiplexing (WDM) return-to- zero signals and demonstrate that both signals at certain power levels have soliton component. We would like to stress that this effect is completely different from the soliton communications studied in the past. Applying Zakharov-Shabat spectral problem to a single WDM or OFDM symbol with multiple sub-carriers we quantify the effect of statistical occurrence of discrete eigenvalues in such an information-bearing optical signal. Moreover, we observe that at signal powers optimal for transmission an OFDM symbol with high probability has a soliton component.

Synthèse du rapport en français

L'équation non linéaire de Schrödinger (NLSE) est souvent utilisée comme modèle maître de moyenne de trajet pour les liaisons par fibre optique afin d'analyser les propriétés fondamentales de ces canaux de communication nonlinéaires. La transmission du signal dans les canaux nonlinéaires est conceptuellement différente des communications linéaires. Nous utilisons ici le modèle de canal NLSE pour expliquer et illustrer certaines nouvelles caractéristiques inhabituelles introduites par la non-linéarité. En général, NLSE décrit la coexistence d'ondes dispersives (continues) et d'ondes localisées (ici dans le temps) - impulsions de soliton. La méthode de la transformée de Fourier non linéaire permet de calculer pour un signal temporel donné le spectre nonlinéaire, qui définit à la fois le spectre continu (analogue à la présentation spectrale de Fourier conventionnelle) et les composantes solitoniques. Le spectre nonlinéaire reste invariant lors de l'évolution du signal dans le canal NLSE. Nous examinons les signaux "return-to-zero" de multiplexage orthogonal de fréquence (OFDM) et multiplexage de longueur d'onde (WDM) et démontrons que les deux signaux à certains niveaux de puissance ont une composante soliton. Nous voudrions souligner que cet effet est complètement différent des communications de solitons étudiées dans le passé. En appliquant le problème spectral de Zakharov-Shabat à un seul symbole WDM ou OFDM avec plusieurs sous-porteuses, nous quantifions l'effet de l'occurrence statistique de valeurs propres discrètes dans un tel signal optique porteur d'informations. De plus, nous observons qu'aux puissances de signal optimales pour la transmission, un symbole OFDM avec une probabilité élevée a une composante soliton.

Contents

List of Figures

Introduction

Fiber-optic communication systems form the basis of the global communication infrastructure, as they provide 99% of the global data traffic. Since fiber optic communication lines appeared in the 1970s, many technological advances such as Erbium-Doped Fiber Amplifiers (EDFA), wavelength division multiplexing (WDM), dispersion control, forward error correction, and gain of Raman scattering, etc., data traffic have grown exponentially. The continuing exponential growth of network traffic is pushing current technology, the data transfer rate of which has increased for several decades, to its limits [1]. Fifth generation optical transmission systems and networks operate with coherent detection, improved multilevel modulation formats and digital signal processing techniques, with channel speeds exceeding 100 Gbit/s. The key to the breakthrough was in reduction of the effects of the most important linear distortion, such as chromatic fiber dispersion and polarization modes. In modern coherent fiber-optic systems, the input signal is reconstructed with the accuracy allowed by channel noise and residual transmission effects that are not compensated by digital signal processing methods. Thus, noise and nonlinearity become key factors that limit the operation of coherent systems.

However, we would like to note that actually chaos based communication has been a very attractive research field from last couple of decades due to its potential of providing secure communication. Moreover, optical chaos is used to synchronization, e.g. synchronization of transmitter and receiver in optical fiber communication systems.

Nonlinear effects in optical fiber are currently the main limiting factor in modern fiber-optic communication systems. Most of the data transmission technologies used today cannot take into account nonlinear effects, since they were originally designed for linear (wired or wireless) communication channels. Therefore, the effect of non-linearity of the fiber, even though it is physically understandable, is often mistakenly perceived as random noise. Over the past 40 years, significant improvements in data transfer rates have been made by incremental changes in the general linear transmission paradigm. Nevertheless, there is much evidence that this trend will end in the next decade. Thus, there is a clear need for radically different approaches to the coding, transmission and processing of information, taking into account the nonlinear properties of optical fiber.

One troubling factor is that the spectral efficiency of fiber-optic channels is limited by existing methods and begins to decrease at high signal powers due to the presence of nonlinearity in fiber. Even with multimode / multi-core fiber optic systems that have recently been proposed as alternatives to increase spectral efficiency, the influence of nonlinearity cannot be avoided. Due to the Kerr effect, the channel spectral efficiency continues to depend on the nonlinear coefficient. Thus, without radical innovations in the physical network infrastructure, we will face what is often called a bandwidth crisis. The recognition of this fact was the point from which the search for alternative solutions began. At present, there is an obvious need for a truly new paradigm of nonlinear communication, including new methods of coding, transmission and processing of information. In other words, the capacity of a nonlinear optical fiber has not yet been fully utilized.

In recent years, considerable efforts have been made to reduce the negative effects of nonlinear fiber using various [2] compensation methods. However, there are numerous problems with the deployment and use of these methods, since most of the technologies used for optical fiber were originally developed for linear channels. Within the framework of such a "linear" ideology, nonlinearity plays the only role of signal distortion. The search for the optimal design of a nonlinear transmission channel and the method of using nonlinearity in a "constructive" manner has a long history. An interesting approach was proposed by Hasegawa and Nyu [3], who investigated the idea of using a nonlinear signal spectrum. This concept is known as "eigenvalue communications" because the information was encoded using discrete eigenvalues (nonlinear spectrum of the Zakharov-Shabat problem) arising from the decomposition of a signal. This idea has recently been used again as a fundamentally new nonlinear communication technique based on the integrability property of the nonlinear channel and the associated nonlinear Fourier transform [4]. The main objective of this proposal is the practical development of the "integrable optical transmission" paradigm for ultrahigh-speed optical communication systems based on the application of nonlinear Fourier transform (NFT) for coding and signal processing. The successful implementation of these ideas should give an unambiguous answer to the questions: "What is the true limit of the bandwidth of a nonlinear fiber channel?" and "How can we achieve this?" . This means that when the constraints associated with "linear methods" decrease, we expect an increase in fiber "productivity" , while nonlinearity works as a constructive element to increase the transmission speed. However, nonlinear effects can be used productively, as they lead to some effects that cannot exist in a linear system. Phase shift, in an optical pulse, due to Cross Phase Modulation (CPM) phenomenon can be used for optical switching; CPM and Self-Phase Modulation (SMP) is able to compress input pulses; Four-wave-mixing (FWM) phenomenon can be used effectively for wavelength conversion.

As part of this work, we are trying to take the first step in the search for the application of nonlinear Fourier transform in modern optical communication lines. The aim of the work

is to apply nonlinear Fourier transform to standard optical signals, such as OFDM and WDM, and to study the characteristics of these signals from the point of view of the nonlinear signal propagation paradigm. The signals are also investigated for the existence of coherent structures in them — solitons, and the criteria for their existence and their influence on the propagation are determined. For the research we use, existing numerical algorithms of nonlinear Fourier transform, as well as their modifications.

The first chapter provides a brief theory of nonlinearity in an optical fiber, describes the theory of integrating the nonlinear Schrödinger equation, and also gives a historical background on the discovery of solitons and their characteristics. Next, the chapter describes the analytical signals for which the scattering data and nonlinear spectra are calculated. Chapter 1 ends with a description of the existing numerical nonlinear Fourier transform algorithms used in the work. The first part of Chapter 2 is devoted to the description of the methodology for the subsequent study of standard optical OFDM and WDM signals. The chapter further describes the formation of the OFDM signal and the results obtained on the dependence of the soliton occurence in the one symbol on the input parameters. Next, the formation of the WDM signal and the corresponding results are described. In conclusion, we describe the prospects for using the nonlinear Fourier transform method for future research.

Part I

Theory

I.1 Nonlinear effects in optical fiber

As in most physical systems, there are observable nonlinear effects in fiber optics, generating phenomena that affect signal propagation and lead to information loss in optical communication lines. The nonlinearity of the fiber is an inherent property of the material environment, depending on the level of transmitted power. An increase in signal power was necessary for the use of WDM systems. The fiber channel capacity becomes limited by fiber nonlinearity as power increases because WDM channel experiences variations of refractive index (through the Kerr nonlinear effect) and becomes distorted. As a consequence, it became necessary to take into account nonlinear effects that become noticeable when the radiation intensity becomes higher than the threshold, as well as during propagation over a long distance, when the influence of nonlinearity of the fiber accumulates.

In an optical fiber, as in a purely nonlinear medium, nonlinear effects may appear. In optical fiber, we can observe the effects of generation of higher optical harmonics, in particular, associated with doubling and tripling of the light frequency; self-focusing and self-channeling phenomena; multiphoton processes (photoionization and photoexcitation, hyper scattering of light, etc.), when not only one, but several photons are involved in the elementary act of the interaction of light with an atom of matter; Kerr effects; Brillouin scattering; Stokes Raman or anti-Stokes Raman scattering, when scattered photon may have lower or higher energy than the incident photon.

The Kerr effect consist of changing the refractive index of the medium under the action of an electric field. In this case, the refractive index will depend on the radiation intensity, and such effects as phase self-modulation, phase cross-modulation, modulation instability, four-wave mixing, and the formation of solitons will occur. For example, the coefficient of nonlinearity of the refractive index for silica fiber is $\approx 2 \cdot 10^{-16}\ \mathrm{W/cm^2}$. Multiplied by intensity, it can already make a significant contribution. The density of light energy currently reaches the

values of $I = 10^7$ W/cm^2. The latter are currently the object of close study, as a result of the newly arisen interest in soliton communication lines. The idea of using such communication lines was proposed in 1973 [5], and after observing optical solitons in 1980 [6], attracted particular attention [7, 8].

I.2 Nonlinear Fourier transform

I.2.1 Nonlinear Schrödinger equation

The method in which the scattered data restore the conditions under which scattering occurred is widely used by scientists in various fields of science. One striking example is the work of Hans Geiger and Ernest Marsden, led by Ernest Rutherford in 1909 to determine the size of an atomic nucleus [9]. In the paper, they bombarded with α-particles a target from several ultrathin layers of gold foil. Finding that some particles deviated at angles greater than 90^o, it was concluded that the mass of the atom is concentrated in a very small positively charged space. With the development of quantum mechanics, the method of determining reflection and transmission coefficients for potential barriers has become an integral part of understanding the principles of operation of quantum systems. Much later, a similar principle began to be used by scientists to solve one-dimensional partial differential equations, where by defining the scattering data in auxiliary problems, one can obtain the necessary solutions to the Cauchy problem for such equations. The method of the inverse scattering problem (IST) perfectly demonstrated its efficiency: in 1967, Gardner [10] described the method of applying this method to the Korteweg-de Vries equation. Many groups of scientists were interested in this method, and a few years later, in 1972, V. Zakharov and A. Shabbat released the work [4], where the IST method was generalized to matrix operators.

A special case of such a problem is the nonlinear (or cubic) Schrödinger equation (NLSE), which is written in the dimensionless form as

$$i\frac{\partial q}{\partial z} + \frac{1}{2}\frac{\partial^2 q}{\partial t^2} + \sigma|q|^2 q = 0, \tag{I.1}$$

where $q(t, z)$ is a complex function that describes the optical signal depending on the time coordinate t and spatial z. According to [11], we use moving frame, where $t = \tau - z/v_g = \tau - \beta_1 z$, v_g is a group velocity. This equation arises when describing various kinds of problems in the study of nonlinear media with dispersion. It describes the wave packet envelope in a medium with dispersion and cubic nonlinearity and is used to describe electromagnetic waves in a plasma, nonlinear crystals, and also to describe signal propagation along an optical fiber.

To go to dimensional units we must make next replacements:

$$\tau = \frac{T}{T_0}t\ , \quad Z = \frac{T^2}{T_0^2}\frac{1}{|\beta_2|}z\ , \quad Q = \sqrt{\frac{|\beta_2|}{\gamma\frac{T^2}{T_0^2}}}q\ , \tag{I.2}$$

as a result of which the equation (I.1) takes the form

$$i\frac{\partial Q}{\partial Z} - \sigma\frac{\beta_2}{2}\frac{\partial^2 Q}{\partial \tau^2} + \gamma|Q|^2 Q = 0. \tag{I.3}$$

Here T is time interval corresponding to the dimensionless interval T_0, β_2 is the group velocity dispersion, γ is the nonlinear Kerr coefficient.

I.2.2 Zakharov-Shabat spectral problem

The main idea of the method proposed by Zakharov and Shabat was to switch from a nonlinear equation to an operator equation of the following form:

$$\frac{\partial L}{\partial z} = [M, L] = ML - LM, \tag{I.4}$$

where M and L are matrix operators of dimension 2×2, and the pair of operators itself is called the Lax pair [12]. We would like to stress that the operator L is an isospectral operator. Finding a Lax pair is a nontrivial task that requires creative thinking and inexhaustible optimism from the researcher, since there is no universal method for finding a pair of operators that satisfy the (I.4) equation and leads to the desired nonlinear equation.

The form of operators M and L for NLSE is known:

$$\mathbf{L} = i\begin{bmatrix} \partial_t & -q(t,z) \\ -\sigma q^*(t,z) & -\partial_t \end{bmatrix} \qquad \mathbf{M} = i\begin{bmatrix} \sigma\frac{\partial^2}{\partial t^2} + \frac{1}{2}|q|^2 & -\sigma q\frac{\partial}{\partial t} - \frac{1}{2}\sigma q_t \\ -q^*\frac{\partial}{\partial t} - \frac{1}{2}q_t^* & -\sigma\frac{\partial^2}{\partial t^2} - \frac{1}{2}|q|^2 \end{bmatrix}$$

where $q(t,z)$ was defined earlier in (I.1).

The equation (I.1) is a compatibility condition for two linear equations:

$$L\Psi = \xi\Psi, \tag{I.5}$$

$$\frac{\partial \Psi}{\partial z} = M\Psi. \tag{I.6}$$

The spectral parameter ξ is generally complex. However, this notation is often used to define a real parameter, and when one want to stress that the parameter is in the upper complex half-plane (as required by causality), the symbol ζ is used. The direct Zakharov-Shabat problem consist of solving a spectral problem for the operator L (I.5), and can be written out as a system

$$\begin{cases} \partial_t\psi_1 = -i\xi\psi_1 + q\psi_2 \\ \partial_t\psi_2 = -\sigma q^*\psi_1 + i\xi\psi_2 \end{cases}. \tag{I.7}$$

or in matrix form

$$\frac{\partial \mathbf{\Psi}(t)}{\partial t} = Q(t,z)\mathbf{\Psi}(t), \tag{I.8}$$

$\mathbf{\Psi}(t)$ — complex vector function of the real variable t, $Q(t,z)$ is a complex matrix that also depends on the complex variable z:

$$\mathbf{\Psi}(t) = \begin{pmatrix} \psi_1(t) \\ \psi_2(t) \end{pmatrix}, \quad Q(t,z) = \begin{pmatrix} -i\xi & q(t,z) \\ -\sigma q^*(t,z) & i\xi \end{pmatrix}. \tag{I.9}$$

In most problems, the variable z is fixed and denoted either as z_0 or $z = 0$, it means that condition is taken at the beginning of the grid. In this case, we can say that the Cauchy problem is posed for the system (I.7) with the initial condition $q(t, z = 0)$, which is the initial field distribution, also called the "scattering potential".

To solve the system (I.7), we assume that $q(t, z_0) = q_0(t)$ is a function that is rapidly decreasing at infinity. We can distinguish two linearly independent solutions as $t \to \pm\infty$:

$$\mathbf{\Phi}_1^- = \begin{bmatrix} 1 \\ 0 \end{bmatrix} e^{-i\xi t} \quad \text{and} \quad \mathbf{\Phi}_2^- = \begin{bmatrix} 0 \\ -1 \end{bmatrix} e^{i\xi t} \quad t \to -\infty, \tag{I.10}$$

$$\mathbf{\Phi}_1^+ = \begin{bmatrix} 1 \\ 0 \end{bmatrix} e^{-i\xi t} \quad \text{and} \quad \mathbf{\Phi}_2^+ = \begin{bmatrix} 0 \\ 1 \end{bmatrix} e^{i\xi t} \quad t \to +\infty. \tag{I.11}$$

We can construct two matrix of fundamental solutions $\Phi^- = (\Phi_1^-, \Phi_2^-)$ and $\Phi^+ = (\Phi_1^+, \Phi_2^+)$, which are connected to each other by the scattering matrix S

$$\Phi^- = \Phi^+ S, \quad S = \begin{pmatrix} a & b^* \\ b & -a^* \end{pmatrix}. \tag{I.12}$$

For real parameters ξ, the coefficients a, b can be defined as follows:

$$\begin{aligned} a(\xi) &= \lim_{t\to\infty} \phi_1(t,\xi) e^{i\xi t}, \\ b(\xi) &= \lim_{t\to\infty} \phi_2(t,\xi) e^{-i\xi t} \end{aligned} \tag{I.13}$$

where the scalar functions $\phi_{1,2}$ are the components of the vector Φ_1^-.

This solution can be interpreted as an abstract wave v^- incident on the potential on the left, partially turning into a wave on the right bv^- with a transmission coefficient $b(\xi)$ and into a wave on the left av^+ with a reflection coefficient $a(\xi)$ (Fig. I.1).

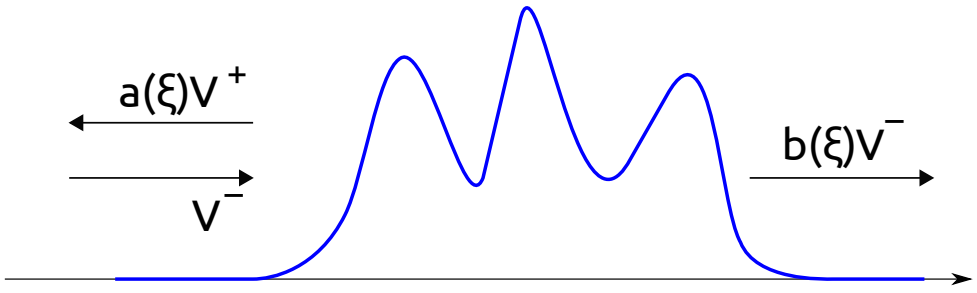

Figure I.1: Scattering example

All spectral data is determined by the coefficients $a(\xi)$ and $b(\xi)$. For a continuous spectrum located on the whole real line, the scattering coefficient is determined by the formula:

$$r(\xi) = \frac{b(\xi)}{a(\xi)}, \quad \xi \in \mathbb{R}. \tag{I.14}$$

For the parameter $\xi = \zeta$, for $\mathrm{Im}\ \zeta > 0$, the zeros of the coefficient $a(\zeta_n)$ determine the discrete spectrum ζ_n, for $n = 1...N$, N is the number of discrete eigenvalues, and the parameter

$$c_n(z) = c(\zeta_n, z) = \frac{b(\zeta_n)}{a'(\zeta_n)}, \quad \text{where} \quad a'(\zeta_n) = \frac{\partial a(\zeta)}{\partial \zeta}|_{\zeta=\zeta_n}, \tag{I.15}$$

is a phase coefficient, which defines complex phase shift for each soliton.

The obtained coefficients are the so-called "scattering data" , which determine the initial potential $q_0(t)$. In order to find the evolution of this data, it is necessary to use the equation (I.6). We can write the result of this calculation in the form of the dependence of the coefficient $b(\xi, z)$ on the variable z:

$$b(\xi, z) = b(\xi, z_0)e^{-2i\xi^2(z-z_0)}, \tag{I.16}$$

expressed in multiplication by the phase factor $e^{-2i\xi^2(z-z_0)}$. The parameter ξ corresponds to both the continuous and discrete spectrum $\xi = \zeta$. Thus, the dependence of the scattering data on z can be represented in the form:

$$r(\xi, z) = r(\xi, z_0)e^{-2i\xi^2(z-z_0)}, \quad c_n(z) = c_n(z_0)e^{-2i\zeta_n^2(z-z_0)}. \tag{I.17}$$

The scattering data forms the core $\Omega(z) = \Omega_{sol}(z) + \Omega_{rad}(z)$, where

$$\Omega_{sol}(z) = \sum_n^N c_n(z)e^{-i\zeta_n t}, \tag{I.18}$$

$$\Omega_{rad}(z) = \frac{1}{2\pi}\int_{-\infty}^{+\infty} d\xi r(\xi, z)e^{-i\xi t1}. \tag{I.19}$$

Here N is a total number of discrete eigenvalues in signal. We want to note the fact that in the absence of a discrete spectrum, the kernel is reduced to (I.19), which is nothing but the Fourier transform.

The final step of the NFT is to restore the signal from the scatter data. In order to restore the signal $q(t, z)$ at the required point z, the obtained core $\Omega(z)$ must be substituted into a pair of integral equations that are called "Gelfand-Levitan-Marchenko equations" (GLM) (see for details e.g. [13]):

$$A_1^*(t, s) + \int_{-s}^{t} \Omega(s + \tau)A_2(t, \tau)d\tau = 0, \tag{I.20}$$

$$-A_2^*(t, s) + \int_{-s}^{t} \Omega(s + \tau)A_1(t, \tau)d\tau + \Omega(t + s) = 0, \tag{I.21}$$

where the parameters are within $-t \leq s < t$ and $0 \leq t \leq T$, $\Omega(t) \equiv \Omega(z = 0, t)$. A pair of functions A_1 and A_2 constitute a solution to the GLM equations. After finding the functions A_1 and A_2, the signal is restored by simple formula

$$q(z, t) = -2A_2^*(t, t). \tag{I.22}$$

I.2.3 Scheme of nonlinear Fourier transform

In conclusion, we summarize the above steps. The nonlinear Fourier transform is an analytical method for solving the Cauchy problem for nonlinear evolution equations. The main stages of the method are illustrated in Fig. I.2:

- Solve the direct scattering problem: for a given initial condition $q(t, 0)$, find the scattering data $\Omega(0)$
- According to $\Omega(0)$, find $\Omega(z)$ using formulas for the evolution of scattering data
- Solve the inverse scattering problem: reconstruct the function $q(t, z)$ from the scattering data $\Omega(z)$ — the solution of the Cauchy problem

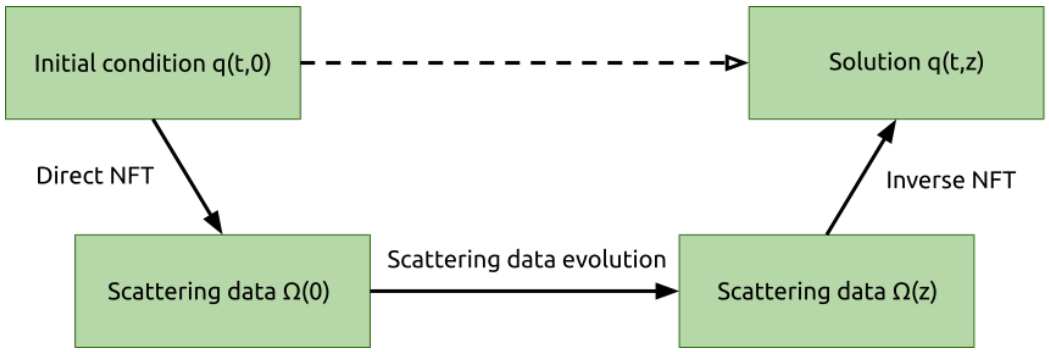

Figure I.2: Scheme of nonlinear Fourier transform

At the first stage, the nonlinear spectrum and the scattering data are determined for a specific initial distribution of the signal $q(t, z_0)$. Depending on the parameter σ, the nonlinear spectrum can contain either only a continuous spectrum lying on the real axis (for $\sigma = -1$), or in addition to the continuous also discrete complex eigenvalues for $\sigma = 1$. In addition, each discrete value corresponds to the soliton contained in the signal under study. It should be noted that in the case of $\sigma = -1$, so-called dark solitons can exist in the signal. They are beyond the scope of this study, therefore are not considered in this paper. At the second stage, the core (I.18) and (I.19) is formed, the evolution of which is calculated by the analytical formula. Finally, the equations (I.20) and (I.21) are solved and the signal $q(t, z)$ is restored by the formula (I.22).

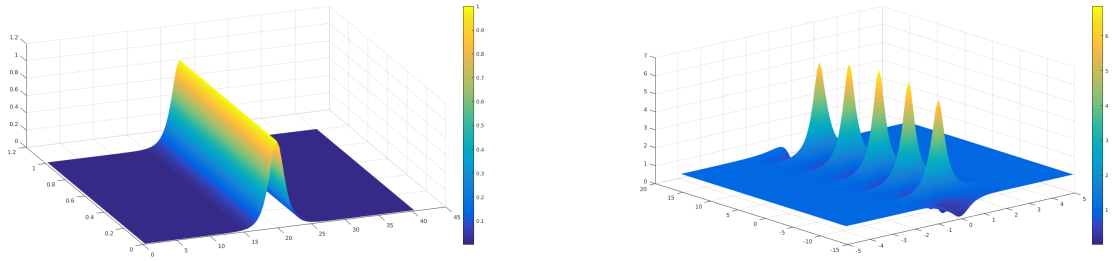

a) b)

Figure I.3: Examples of soliton solution: a) — fundamental soliton, b) — Akhmediev breather.

I.2.4 Solitons

The history of solitons begins in fact in 1834, when James Scott Russell observed a solitary shaft of water in a channel, moving without a noticeable change in shape or decrease in speed over several kilometers [14]. Such waves were called solitary, and later, in 1965, the term soliton was introduced to represent their particle-like essence [15]. However, even earlier, in 1831, M. Faraday [16] described an effect in which a fine powder placed on an oscillating surface gathered in small "heaps" , which could be both stationary and moving. The properties of solitons were studied in the 1960s, when the inverse scattering method was introduced, in which solitons arose as separate solutions [10].

In the 20th century, autosolitons (dissipative solitons) were actively studied in physical, chemical, and biological systems. The main work on this topic is related to the reaction-diffusion model [17, 18], which describes the localized structures that arise in the chemical reactions of activators, or in current flows in plasma, gas and semiconductors.

In nonlinear optics, solitons are divided into temporal and spatial. The temporal solitons are localized in time and related to optical pulses that retain their shape, and the spatial ones are self-directed beams, limited in transverse directions, orthogonal to the propagation vector. The formation and existence of such types of solitons is caused by the optical Kerr effect [19, 20, 21] — a nonlinear change in the refractive index of the medium, depending on the light intensity and leading to spatial focusing (or defocusing) and temporal self-modulation phase.

Optical solitons are divided into two large classes: conservative and dissipative. Conservative solitons are created due to the balance of nonlinear focusing and linear spreading in transparent media in which there is no energy pumping, and the radiation loss is negligible. Dissipative solitons (autosolitons) are localized as a result of the balance of the inflow and outflow of energy in the system. For them, there may also be an effect of balancing linear spreading and nonlinear focusing.

These two classes of solitons have both common properties and fundamental differences,

as a result of their common nature, but of a different method of formation. The set of basic parameters of dissipative solitons is discrete due to the requirement for the energy balance. This leads to their increased stability, and, as a result, dissipative solitons have prospects in various practical applications. Conservative solitons are determined by a continuously varying parameter, for example, intensity or width. Depending on the method of energy input into the optical system, the solitons are divided into coherent and incoherent. Coherent solitons are formed in a beam of continuous coherent radiation, which determines the frequency and phase. The incoherent signal forms incoherent solitons, for which the common radiation phase is arbitrary.

Due to the presence of noise in real systems, the possibility of spontaneous transition between soliton and soliton-free structures is realized. The soliton itself, although not a stable structure, can exist for a long time, since it is resistant to small perturbations. Transitions can be caused by large fluctuations that are unlikely in real systems. This fact leads to one interesting feature described in [22], when in the process of signal evolution in the system solitons arise.

The study of optical solitons began in the 60s of the 20th century, when the first optical nonlinear systems appeared, and experiments in this field became available. The first example was the article [23] about the possibility of the existence of a spatial conservative soliton in a transparent medium with a self-focusing nonlinearity. Later, a time soliton was discovered in single-mode fibers with the Kerr nonlinearity [5].

I.2.5 Analytical solutions

Satsuma-Yajima signal

As the first analytical signal for which the nonlinear spectrum is known, we take the following:

$$q(t,0) = A\ \mathrm{sech}(t), \tag{I.23}$$

hyperbolic profile with variable amplitude A. We assume that $A > 0$ is real, because otherwise the phase factor only affects the phase of the solution $q(t,z)$, which in this context does not interest us. In 1974, Satsuma and Yajima showed that the signal (I.23) is a particular solution of the Zakharov-Shabat problem (I.7), and its nonlinear spectrum was found.

They found that the function written as follows:

$$\psi_1(t;\zeta) = \begin{pmatrix} y_1^{(1)}(s;\zeta) \\ -A(\zeta - \frac{1}{2}i)^{-1} y_1^{(2)}(s;-\zeta) \end{pmatrix}, \tag{I.24}$$

is the Jost function of the problem (I.7), where the functions $y_1^{(1,2)}$ are defined by:

$$y_1^{(1)}(s;\zeta) = s^{i\zeta/2}(1-s)^{-i\zeta/2} F\left(-A, A, i\zeta + \frac{1}{2}; s\right) \tag{I.25}$$

$$y_1^{(2)}(s;\zeta) = s^{1/2-i\zeta/2}(1-s)^{-i\zeta/2}F\left(\frac{1}{2}-i\zeta+A, \frac{1}{2}-i\zeta-A, \frac{3}{2}-i\zeta; s\right) \tag{I.26}$$

in which $F(\alpha,\beta,\gamma;s)$ is a hypergeometric function, $s \equiv \frac{1-\tanh(x)}{2}$. Taking into account the properties of the hypergeometric function:

$$F(\alpha,\beta,\gamma;0) = 1$$

$$F(\alpha,\beta,\gamma;s) = \frac{\Gamma(\gamma)\Gamma(\gamma-\alpha-\beta)}{\Gamma(\gamma-\alpha)\Gamma(\gamma-\beta)}F(\alpha,\beta,\alpha+\beta+1-\gamma;1-s) + \\ + \frac{\Gamma(\gamma)\Gamma(\alpha+\beta-\gamma)}{\Gamma(\alpha)\Gamma(\beta)}(1-s)^{\gamma-\alpha-\beta}F(\gamma-\alpha,\gamma-\beta,1+\gamma-\alpha-\beta;1-s)$$

it is easy to calculate the asymptotic behavior of the function $\psi_1(t;\zeta)$:

$$\psi_1(t;\zeta) \to \begin{pmatrix}1\\0\end{pmatrix} e^{-i\zeta t}, \qquad x \to \infty \tag{I.27}$$

$$\psi_1(t;\zeta) \to \begin{pmatrix}\frac{\Gamma^2(i\zeta+\frac{1}{2})}{\Gamma(i\zeta+\frac{1}{2}+A)\Gamma(i\zeta+\frac{1}{2}-A)}e^{-i\zeta t}\\ -i\sin(\pi A)\mathrm{sech}(\pi\zeta)e^{i\zeta t}\end{pmatrix}, \qquad x \to -\infty \tag{I.28}$$

The function $\frac{\Gamma^2(i\zeta+\frac{1}{2})}{\Gamma(i\zeta+\frac{1}{2}+A)\Gamma(i\zeta+\frac{1}{2}-A)}$ in front of $e^{-i\zeta t}$ in the last expression is nothing more than the coefficient $a(\zeta)$ whose zeros give us a discrete spectrum for problem (I.7):

$$\zeta_n = i\left(A+\frac{1}{2}-n\right), \tag{I.29}$$

where n is a positive integer satisfying the condition $n < A+\frac{1}{2}$. The first eigenvalue appears at $A = \frac{1}{2}$, the second at $A = \frac{3}{2}$ and so on. Thus, for an arbitrary $A > 0$, the number of discrete eigenvalues is equal to the largest integer number n satisfying the condition $n - \frac{1}{2} < A$.

Rectangular pulse

Another example of the initial distribution is a rectangular pulse with varying amplitude:

$$q(t,0) = \begin{cases} A, & 0 \le t \le 1, \\ 0, & \text{otherwise.} \end{cases} \tag{I.30}$$

Similarly, with the previous type of signal, we assume that $A > 0$ and real. The coefficient $a(\zeta)$ takes the form:

$$a(\zeta) = e^{i\zeta}\left(\cos\sqrt{\zeta^2+A^2} - \frac{i\zeta}{\sqrt{\zeta^2+A^2}}\sin\sqrt{\zeta^2+A^2}\right). \tag{I.31}$$

This expression is zero if the expression in parentheses is zero, which leads us to the transcendental equation:

$$\cot\sqrt{\zeta^2+A^2}=\frac{i\zeta}{\sqrt{\zeta^2+A^2}} \tag{I.32}$$

This expression can be satisfied only for imaginary ζ. Each subsequent eigenvalue appears when $A=(n-\frac{1}{2})\pi$, where n is a positive integer. This formula can be rewritten as

$$N=\mathrm{int}[1/2+L_1(q)/\pi], \tag{I.33}$$

where $\mathrm{int}[...]$ means the integer part of the expression in brackets, and N is the number of solitons. The first level L_1 of the norm calculated by this formula is 1.57, the second is 4.71 and so on.

I.2.6 The criteria for the existence of discrete eigenvalues

Above, we saw that there is a criteria for signals of a certain form, which determines the possibility of the existence of discrete eigenvalues in the Zakharov-Shabat problem. The imprecise criterion described in [24] is that if L_1 norm, defined by the formula

$$L_1(q)=\|q(t,0)\|_{L_1}=\int\limits_{-\infty}^{+\infty}|q(t,0)|dt \tag{I.34}$$

(where $q(t,z)$ is signal to study, t and z — time and space coordinates), is less than 1.317, then the system (I.7) does not have a discrete spectrum.

Later, in 2003, Klaus and Shaw found an exact criterion in [25]. For the complex initial condition $q(t,0)$, there is no discrete spectrum if

$$\|q(t,0)\|_{L_1}\leq\frac{\pi}{2}. \tag{I.35}$$

If L_1 norm is greater than a given value, then a discrete spectrum may exist (but not necessarily exist).

In this paper we use both the L_1 norm (I.34) and the L_2 norm

$$L_2(q)=\|q(t,0)\|_{L_2}=\int\limits_{-\infty}^{+\infty}|q(t,0)|^2dt, \tag{I.36}$$

for which there is no criterion like (I.35). However, for numerical simulation, we can obtain a criterion that can give us some preliminary information about the L_2 levels of the norm, and therefore about the average signal power, less than which there cannot be any discrete spectrum in the signals. Without loss of generality, we consider the signal $q(t,z)$ for a fixed spatial coordinate z. Subsequent calculations are performed in dimensionless units.

$$L_1 = \|q(t,z)\|_{L_1} = \sum_{n=0}^{N-1} |q_n| \Delta t, \tag{I.37}$$

$$L_2 = \|q(t,z)\|_{L_2} = \sum_{n=0}^{N-1} |q_n|^2 \Delta t, \tag{I.38}$$

where $\Delta t = T/N$, T is the time interval on which the function $q(t,z)$ is defined, N is the number of sampling points, q_n are the values of the function $q(t_n,z)$ at these points. Since we have some finite set of q_n values, we can calculate the average value for this set

$$< |q_n| >= \frac{1}{N} \sum_{n=0}^{N-1} |q_n| = \frac{L_1}{N\Delta t} = \frac{L_1}{T}, \tag{I.39}$$

$$< |q_n|^2 >= \frac{1}{N} \sum_{n=0}^{N-1} |q_n|^2 = \frac{L_2}{N\Delta t} = \frac{L_2}{T}, \tag{I.40}$$

where the brackets $< ... >$ denote the operation of taking the average. The modulus of complex numbers is real and satisfies the condition $|q_n| \geq 0$. Also the value of L_1 is equal to or greater than 0 by definition. Now remember that the average of the square of a positive value is greater than or equal to the square of the average of this value (generalized mean inequality), one can write

$$< |q_n|^2 > \geq < |q_n| >^2 \quad \Rightarrow \quad \frac{L_2}{T} \geq \frac{L_1^2}{T^2}. \tag{I.41}$$

It remains to obtain the constraint on L_1^2 from the criterion I.35). First of all, we note that $\frac{\pi}{2} > 1$, which implies

$$L_1 > \frac{\pi}{2} \quad \Rightarrow \quad L_1^2 > \frac{\pi^2}{4} \quad \Rightarrow \quad \frac{L_1^2}{T} > \frac{\pi^2}{4T}. \tag{I.42}$$

We can conclude that the criterion for the existence of discrete eigenvalues of the Zakharov-Shabat problem for the L_2 norm:

$$L_2 > \frac{\pi^2}{4T}. \tag{I.43}$$

It is not surprising that in the limit $T \to \infty$ the criterion reduces to a simple $L_2 > 0$. However, in most problems, the signal is localized in time, so the integral over an infinite interval in the formula (I.36) can be replaced by an integral over a finite interval, where the signal is not zero

$$\widetilde{L_2} = \|q(t,z)\|_{\widetilde{L_2}} = \int_{-T/2}^{T/2} |q(t,z)|^2 dt, \tag{I.44}$$

for which the criterion (I.43) works.

I.3 Methods for numerical calculations

I.3.1 Boffetta-Osborne method for determining scattering data

This method was proposed in 1992 by Boffetta and Osborne and described in detail in their work [26]. The main idea of the method is that the ZS system can be rewritten as:

$$\begin{cases} \partial_t \psi_1 = -\xi\psi_1 + q\psi_2 \\ \partial_t \psi_2 = \sigma q^* \psi_1 + \xi\psi_2 \end{cases} \tag{I.45}$$

which, after passing to a discrete grid for t variable, gives an evolution of the spectral eigenfunction Ψ on each interval Δt:

$$\Psi(t_n + \Delta t) = U(q_n)\Psi(t_n) \tag{I.46}$$

where $U(q_n, \Delta t)$ is represented as an exponential function of the matrix $Q(\xi)$:

$$U(q) = \exp[\Delta t Q(\xi)] = \exp\left(\Delta t \begin{pmatrix} -i\xi & q \\ \sigma q^* & i\xi \end{pmatrix}\right) \tag{I.47}$$

If we expand the above exponent into a Taylor series and sum up the matrices, and then, assuming that each element of the matrix is a Taylor series, we summarize these rows for each element, then we get the following expression for the propagator:

$$\begin{aligned} U(q) &= \exp[\Delta t Q(\xi)] = \\ &= \begin{pmatrix} \cosh(k\Delta x) - \frac{i\xi}{k}\sinh(k\Delta x) & \frac{q}{k}\sinh(k\Delta x) \\ \frac{\sigma q^*}{k}\sinh(k\Delta x) & \cosh(k\Delta x) + \frac{i\xi}{k}\sinh(k\Delta x) \end{pmatrix} \end{aligned} \tag{I.48}$$

where $k^2 = \sigma|q|^2 - \xi^2$ is a constant on the interval Δt. Using the above method, we can solve the scattering problem — determine the coefficients $a(\xi)$ and $b(\xi)$. However, for a discrete spectrum, this is not sufficient: since the coefficient $a(\xi)$ is zero, it is necessary to calculate its derivative $a'(\xi_n) = \frac{\partial a(\xi)}{\partial \xi}|_{\xi=\xi_n}$. Now we introduce a four-component field containing both the vector function Ψ and its derivative with respect to ξ:

$$\Xi(t, \xi) = \begin{pmatrix} \Psi \\ \Psi' \end{pmatrix} \tag{I.49}$$

where $\Psi' = \partial\Psi/\partial\xi$. Similar to the expressions (I.47) and (I.48) for the Ξ field, one can write a recursive relation by differentiating the expression (I.46):

$$\Xi(t_n + \Delta t) = T(q_n)\Xi(t_n) \tag{I.50}$$

here

$$T(q_n) = \begin{pmatrix} U(q_n) & 0 \\ U'(q_n) & U(q_n) \end{pmatrix} \tag{I.51}$$

4×4 matrix, $U'(q_n) = \partial U(q_n)/\partial\xi$ and can be written as:

$$\begin{aligned} U'_{11} &= i\Delta t\frac{\xi^2}{k^2}\cosh(k\Delta t) - \left(\xi\Delta t + i + i\frac{\xi^2}{k^2}\right)\frac{\sinh(k\Delta t)}{k} \\ U'_{12} &= -\frac{q\xi}{k^2}\left(\Delta t\cosh(k\Delta t) - \frac{\sinh(k\Delta t)}{k}\right) \\ U'_{21} &= -\frac{\sigma q\xi}{k^2}\left(\Delta t\cosh(k\Delta t) - \frac{\sinh(k\Delta t)}{k}\right) \\ U'_{22} &= -i\Delta t\frac{\xi^2}{k^2}\cosh(k\Delta t) - \left(\xi\Delta t - i - i\frac{\xi^2}{k^2}\right)\frac{\sinh(k\Delta t)}{k} \end{aligned} \tag{I.52}$$

For the numerical calculation, we consider the initial potential of $q(t,0)$ on the $M+1$ segments, assuming that

$$q(t,0) = q_n \quad \text{when} \quad t \in \left(t_n - \frac{\Delta t}{2};\ t_n + \frac{\Delta t}{2}\right]. \tag{I.53}$$

In this case, the discrete solution of the scattering problem is the following:

$$\Xi(t_n) = \prod_{j=n-1}^{-M/2} T(q_j)\Xi(t_{-M/2}). \tag{I.54}$$

To obtain the scattering data, it is necessary to calculate the scattering matrix S

$$S(\xi) = \prod_{j=M/2-1}^{-M/2} T(q_j) = \begin{pmatrix} \Sigma(\xi) & 0 \\ \Sigma'(\xi) & \Sigma(\xi) \end{pmatrix}, \tag{I.55}$$

where matrix Σ is defined as

$$\Sigma = \prod_{j=M/2-1}^{-M/2} U(q_j), \quad \Sigma' = \partial\Sigma/\partial\xi. \tag{I.56}$$

Initially, in the problem (I.7), the vector function Ψ extended from $-\infty$ to $+\infty$. In numerical simulation, this interval is replaced by the interval from $-\frac{T}{2}$ to $+\frac{T}{2}$. In this case, we get the following result:

$$\begin{aligned} a(\xi) &= S_{11}(\xi)e^{i\xi T}, \\ b(\xi) &= S_{21}(\xi), \\ \frac{\partial a(\xi)}{\partial\xi} &= [S_{31} + i\frac{T}{2}(S_{11} + S_{33})]e^{i\xi T}, \\ \frac{\partial b(\xi)}{\partial\xi} &= S_{41} + i\frac{T}{2}(S_{43} - S_{21}). \end{aligned} \tag{I.57}$$

This method allows us to find all the scattering data for an arbitrary ξ. Although the method does not directly calculate the spectrum of the problem (I.7), it can help us find it, because we know that at the points of the discrete spectrum on the complex plane the scattering coefficient $a(\xi) \equiv 0$.

It should be noted that for $t \ll 1$ the matrix $U(q)$ I.48 reduces to

$$U(q) \approx \begin{pmatrix} 1 - i\xi\Delta t & q\Delta t \\ \sigma q^* \Delta t & 1 + i\xi\Delta t \end{pmatrix}. \tag{I.58}$$

This form was found by Ablowitz and Ladik [27, 28] and can also be used to solve the Zakharov-Shabat problem.

I.3.2 Töplitz inner bordering method

The formation of technologies for creating fiber Bragg gratings (FBGs) [29, 30] was accompanied by the development of numerical methods for their modeling and analysis. Recovery of the refractive index from a given dependence of the scattering coefficient on the frequency is the inverse scattering problem, which is solved in mathematical physics using a pair of Gelfand-Levitan-Marchenko [4] equations.

The work [31] was proposed a method for solving the GLM equations (I.20) and (I.21). It consists in the fact that the GLM equations can be reduced to equations with the Toeplitz kernel by replacing $u(t,x) = A_1(t, t-x)$ and $v(t,y) = -A_2^*(t, y-t)$:

$$\begin{aligned} u(t,x) + \int_x^{2t} \Omega^*(y-x)v(t,y)dy = 0 \\ v(t,y) + \int_0^{y} \Omega(y-x)u(t,x)dx + \Omega(y) = 0 \end{aligned} \tag{I.59}$$

where $\Omega = \Omega_{sol} + \Omega_{rad} = \sum\limits_n c_n e^{-i\xi_n x} + \frac{1}{2\pi}\int\limits_{-\infty}^{+\infty} d\xi r(\xi) e^{-i\xi x}$ — integral kernel, the parameters x and y are in the range $0 \leq x,y < 2t$, the variable t is in the range $0 \leq t < T$, and the signal is restored using the formula $q(t) = 2v(t, 2t-0)$.

Further, the equations (I.59) are discretized on a uniform grid, and the integrals are represented as sums. The resulting equations have a block structure and are written in matrix form:

$$\mathbf{G}\begin{pmatrix} \mathbf{u} \\ \mathbf{v} \end{pmatrix} = \begin{pmatrix} \mathbf{a} \\ \mathbf{b} \end{pmatrix} \tag{I.60}$$

where matrix $\mathbf{G}$ and vectors $\mathbf{u}$, $\mathbf{v}$, $\mathbf{a}$ and $\mathbf{b}$ are defined by:

$$\mathbf{G} = \begin{pmatrix} \mathbf{E} & \pm\mathbf{\Omega}^{\dagger} \\ \mathbf{\Omega} & \mathbf{E} \end{pmatrix}, \quad \mathbf{\Omega} = h \begin{pmatrix} \frac{1}{2}\Omega_0 & 0 & \dots & 0 \\ \Omega_1 & \frac{1}{2}\Omega_0 & \dots & 0 \\ & & \ddots & \\ \Omega_{m-1} & \Omega_{m-2} & \dots & \frac{1}{2}\Omega_0 \end{pmatrix}$$

$$\mathbf{a} = \pm\frac{h}{2} v_m^{(m)} \tilde{\rho}^*, \mathbf{b} = -\left(1 + \frac{h}{2} u_1^{(m)} \rho\right),$$

$$\rho = \begin{pmatrix} \Omega_1 \\ \vdots \\ \Omega_m \end{pmatrix}, \mathbf{u} = \begin{pmatrix} u_1^{(m)} \\ \vdots \\ u_m^{(m)} \end{pmatrix}, \mathbf{v} = \begin{pmatrix} v_1^{(m)} \\ \vdots \\ v_m^{(m)} \end{pmatrix}. \tag{I.61}$$

$\mathbf{E}$ — identity matrix.

The first and last elements of the solution vector are calculated by the formulas:

$$u_1^{(m)} = \pm\frac{h}{2} v_m^{(m)} \langle \mathbf{y}^* | \tilde{\rho}^* \rangle \mp \left(1 + \frac{h}{2} u_1^{(m)}\right) \langle \mathbf{z}^* | \rho \rangle,$$

$$u_1^{(m)} = \pm\frac{h}{2} v_m^{(m)} \langle \tilde{\mathbf{z}} | \tilde{\rho}^* \rangle - \left(1 + \frac{h}{2} u_1^{(m)}\right) \langle \tilde{\mathbf{y}} | \rho \rangle. \tag{I.62}$$

Parentheses denote scalar product $\langle \mathbf{x} | \mathbf{y} \rangle = \mathbf{x}^T \cdot \mathbf{y}$. We can introduce the following parameters

$$\alpha_m = h \langle \mathbf{z}^* | \rho \rangle, \quad \beta_m = h \langle \tilde{\mathbf{y}} | \rho \rangle. \tag{I.63}$$

Then equation (I.62) allows calculate $v_m^{(m)}$:

$$v_m^{(m)} = \frac{-\beta_m / h}{1 \pm \operatorname{Im}\, \alpha_m - \frac{1}{4}(|\alpha_m|^2 \mp |\beta_m|^2)}. \tag{I.64}$$

We assume that with the required accuracy $\alpha_m = -u(x_m, 0)h + O(h^2)$, which leads us to the final solution:

$$q_m = 2v_m^{(m)} = -2\beta_m / h + O(h^2). \tag{I.65}$$

This procedure can be described as an algorithm that can be reversed. Next, we present two algorithms of direct and inverse transformations, as a result of which a signal can be reconstructed from the core (Algorithm 1) and vice versa: the integral core is obtained from the signal (Algorithm 2).

I.3.3 N-soliton solution

Factorization of GLM equations

For a discrete spectrum, factorization of the kernel of the GLM equations leads to a system of algebraic equations (a detailed description can be found in [32]). Then the N-soliton solution

Algorithm 1. Inverse TIB algorithm for signal recovery from the kernel

1: $m = 1$ $q_0 = -2\Omega_0$ $y_0^{(1)} = \frac{1}{1 \mp h^2|\Omega_0|^2/4}$ $z_0^{(1)} = -\frac{y_0^1 h \Omega_0}{2}$

2: $\beta_m = h \sum_{j=0}^{m-1} \Omega_{m-j} y_j^{(m)}$

3: $q_m = -2\beta_m / h$

4: $c_m = \frac{1}{1 \mp |\beta_m|^2}, d_m = -\beta_m c_m$

5: $\mathbf{y}^{(m+1)} = c_m \begin{pmatrix} \mathbf{y}^{(m)} \\ 0 \end{pmatrix} + d_m \begin{pmatrix} 0 \\ \pm \tilde{\mathbf{z}}^{*(m)} \end{pmatrix}$

6: $\mathbf{z}^{(m+1)} = c_m \begin{pmatrix} \mathbf{z}^{(m)} \\ 0 \end{pmatrix} + d_m \begin{pmatrix} 0 \\ \tilde{\mathbf{y}}^{*(m)} \end{pmatrix}$

7: Increment m, go to the step 2.

Algorithm 2. TIB direct algorithm for calculating the kernel from the signal

1: $\Omega_0 = -q_0/2$

2: $\beta_m = -h q_m / 2$

3: $\Omega_m = \left(\beta_m - h \sum_{j=1}^{m-1} R_{m-j} y_j^{(m)} \right) / h y_0^{(m)}$

4: $c_m = \frac{1}{1 \mp |\beta_m|^2}, d_m = -\beta_m c_m$

5: $\mathbf{y}^{(m+1)} = c_m \begin{pmatrix} \mathbf{y}^{(m)} \\ 0 \end{pmatrix} + d_m \begin{pmatrix} 0 \\ \pm \tilde{\mathbf{z}}^{*(m)} \end{pmatrix}$

6: $\mathbf{z}^{(m+1)} = c_m \begin{pmatrix} \mathbf{z}^{(m)} \\ 0 \end{pmatrix} + d_m \begin{pmatrix} 0 \\ \tilde{\mathbf{y}}^{*(m)} \end{pmatrix}$

7: Increment m, go to the step 2.

can be found using the following exact expression:

$$q^{(N)}(t, z=0) = -2\langle \mathbf{\Psi}(t)|(\widehat{\mathbf{E}} + \widehat{\mathbf{M}}^*(t)\widehat{\mathbf{M}}(t))^{-1}|\mathbf{\Phi}(t)\rangle \tag{I.66}$$

$\widehat{\mathbf{E}}$ is $N \times N$ identity matrix,

$$\begin{aligned} \langle \mathbf{\Psi}(t)| &= \langle c_1 e^{-i\xi_1 t}, ..., c_N e^{-i\xi_N t}|, \\ \langle \mathbf{\Phi}(t)| &= \langle e^{-i\xi_1 t}, ..., e^{-i\xi_N t}|, \\ \widehat{\mathbf{M}}_{k,j}(t) &= c_j \frac{e^{i(\xi_k^* - \xi_j)t}}{\xi_k^* - \xi_j}, \end{aligned} \tag{I.67}$$

c_j were defined in (I.15). For large N, numerical algorithms for this formula are unstable, but for small N this method is very convenient. For the numerical inversion of matrices, $O(n^4)$ operations are required in the general case. Special algorithms require $O(n^3)$ operations. The process accumulates a calculation error and we cannot find a solution for large N ($N > 100$).

Recursive Darboux method

There is another method to find the N-soliton solution, which is called the dressing method. The main idea of the method is to use the Darboux transformation, which is used to construct an iterative scheme for finding the N-soliton solution. Consider this method in more detail.

Let us introduce the following system:

$$\begin{cases} x_t = P(\zeta, q)x, \\ x_z = M(\zeta, q)x, \end{cases} \tag{I.68}$$

where operator M is defined in (I.6), and P is calculated by the formula

$$P = \begin{pmatrix} -i\lambda & q(t,z) \\ -q^*(t,z) & i\lambda \end{pmatrix}. \tag{I.69}$$

This is the same $Q(t, z)$ matrix from the expression (I.9), but with $\sigma = 1$, since we study soliton solutions. Also, we use the notation $\xi = \lambda$ — a complex number, but not necessarily an eigenvalue for q, which is the solution underlying the system (I.68).

Theorem (Darboux transformation). Let $\phi(t, \lambda; q)$ be a known solution of (I.68), and $\Sigma = S\Gamma S^{-1}$, where $S = [\phi(t, \lambda; q), \tilde{\phi}(t, \lambda; q)]$, $\Gamma = \mathrm{diag}(\lambda, \lambda^*)$. If $v(t, \mu; q)$ satisfies (I.68), then $u(t, \mu; \tilde{q})$, obtained from the Darboux transform

$$u(t, \mu; \tilde{q}) = (\mu I - \Sigma)v(t, \mu; q), \tag{I.70}$$

satisfies (I.68) as well, for

$$\tilde{q} = q + 2i(\lambda^* - \lambda)\frac{\phi_1 \phi_2^*}{|\phi_1|^2 + |\phi_2|^2}. \tag{I.71}$$

Futhermore, q and $\tilde{q}$ satisfy the integrable equation underlying the system (I.68).

From this theorem follows:

- From $\phi(t,\lambda;q)$ and $v(t,\mu;q)$ one can construct $u(t,\mu;\tilde{q})$. If μ is an eigenvalue of q, then it is an eigenvalue of $\tilde{q}$ as well. If $u(t,\mu=\lambda;\tilde{q})\neq 0$, so λ is also an eigenvalue of $\tilde{q}$.
- $\tilde{q}$ is a new solution underlying (I.68), obtained from q according to (I.71), and $u(t,\mu;\tilde{q})$ is one of its eigenvectors.

The algorithm begins with a trivial solution $q^{(0)}=0$, and the initial eigenvectors are chosen as $v(t,\lambda_j;0)=[A_j e^{-i\lambda_j t}, B_j e^{i\lambda_j t}]$. The coefficients A_j and B_j determine the spectral amplitude and shape of the pulse. In order to get new eigenvectors, one needs to use the following formulas:

$$\begin{aligned} v_1(t,\lambda_j;q^{(k+1)}) =& \frac{1}{\|v(t,\lambda_{k+1};q^{(k)})\|^2} \\ & \{\{(\lambda_j-\lambda_{k+1})|v_1(t,\lambda_{k+1};q^{(k)})|^2+ \\ & +(\lambda_j-\lambda_{k+1}^*)|v_2(t,\lambda_{k+1};q^{(k)})|^2\}v_1(t,\lambda_j;q^{(k)}) \\ & (\lambda_{k+1}^*-\lambda_{k+1})v_1(t,\lambda_{k+1};q^{(k)})v_2^*(t,\lambda_{k+1};q^{(k)})v_2(t,\lambda_j;q^{(k)})\}, \end{aligned} \tag{I.72}$$

$$\begin{aligned} v_2(t,\lambda_j;q^{(k+1)}) =& \frac{1}{\|v(t,\lambda_{k+1};q^{(k)})\|^2} \\ & \{\{(\lambda_j-\lambda_{k+1}^*)|v_1(t,\lambda_{k+1};q^{(k)})|^2+ \\ & +(\lambda_j-\lambda_{k+1})|v_2(t,\lambda_{k+1};q^{(k)})|^2\}v_2(t,\lambda_j;q^{(k)}) \\ & (\lambda_{k+1}^*-\lambda_{k+1})v_1^*(t,\lambda_{k+1};q^{(k)})v_2(t,\lambda_{k+1};q^{(k)})v_1(t,\lambda_j;q^{(k)})\}, \end{aligned} \tag{I.73}$$

for $k=0,...,N-2$ and $j=k+2,...,N$. A signal addition occurs according to the formula:

$$q^{(k+1)}=q^{(k)}+2i(\lambda_{k+1}^*-\lambda_{k+1})\frac{v_1(t,\lambda_{k+1};q^{(k)}}{\|v(t,\lambda_{k+1};q^{(k)})\|^2} \tag{I.74}$$

Such a method is convenient for obtaining N-soliton solutions with a large value of N, since matrices are not required to be inverted.

I.3.4 Fourier collocation method for finding a nonlinear spectrum

For most of the initial potentials, the nonlinear spectrum cannot be calculated analytically. In such cases, it is necessary to use numerical algorithms.

The equation (I.5) is a standard problem of finding the eigenvalues of the operator L and is represented as a system:

$$\begin{cases} -\partial_t\psi_1+q(t,0)\psi_2=\xi\psi_1 \\ \partial_t\psi_2-\sigma q^*(t,0)\psi_1=\xi\psi_2. \end{cases} \tag{I.75}$$

One way to solve this problem is to move to finite difference schemes on a discrete grid. For this, a finite interval is selected from the infinite interval along the t axis and is divided into finite intervals, in accordance with the sampling grid. Derivatives operators are replaced by their finite-difference analogues. After these operations, the problem (I.5) becomes the standard task of finding eigenvalues and eigenfunctions for matrices, which can be solved by standard algorithms: LR, QR, the Cholesky method and so on. It should be noted that the QR-algorithm is more stable than the LR, which is now almost not used. Unfortunately, the accuracy of approximation by means of the finite-difference method is rather low and can lead to the appearance of "spurious" eigenvalues.

We can assume that if we could rewrite the original system (I.75) without differential operators, then we could use this method to find the nonlinear spectrum. In this question, the classical Fourier transform helps us, in which differential operators are replaced with multiplication by the appropriate factor:

$$\begin{cases} -\partial_t \psi_1 + q(t,0)\psi_2 = \xi\psi_1 \\ \partial_t \psi_2 - \sigma q^*(t,0)\psi_1 = \xi\psi_2 \end{cases} \rightarrow \begin{cases} -ik\phi_1 + u\phi_2 = \xi\phi_1 \\ ik\phi_2 - \sigma u^*\phi_1 = \xi\phi_2 \end{cases} \tag{I.76}$$

In this transform, we replace the initial potential and eigenfunctions with the following discrete sums:

$$\psi_1(t) = \sum_{-N/2}^{N/2} \phi_{1,n} e^{ink_0 t}, \psi_2(t) = \sum_{-N/2}^{N/2} \phi_{2,n} e^{ink_0 t}, q(t,0) = \sum_{-N/2}^{N/2} u_n e^{ink_0 t}, \tag{I.77}$$

where $k_0 = 2\pi/T$, T is a time slot and $N+1$ is a number of discretization points (number of Fourier modes) in the Fourier transform of the initial signal $q(t,0)$ (N is even). With this transform, the initial problem (I.75) is replaced by the problem of finding eigenvalues for a block matrix:

$$\begin{pmatrix} -H_1 & H_2 \\ H_2^\dagger & H_1 \end{pmatrix} \begin{pmatrix} \phi_1 \\ \phi_2 \end{pmatrix} = i\xi \begin{pmatrix} \phi_1 \\ \phi_2 \end{pmatrix}, \tag{I.78}$$

where

$$\begin{aligned} \phi_1 &= (\phi_{1,-N/2}, \phi_{1,-N/2+1}, ..., \phi_{1,N/2-1}, \phi_{1,N/2})^T \\ \phi_2 &= (\phi_{2,-N/2}, \phi_{2,-N/2+1}, ..., \phi_{2,N/2-1}, \phi_{2,N/2})^T \end{aligned} \tag{I.79}$$

The blocks of the matrix are as follows:

$$H_1 = ik_0 \begin{pmatrix} -\frac{N}{2} & & & & \\ & -\frac{N}{2}+1 & & & \\ & & \ddots & & \\ & & & \frac{N}{2}-1 & \\ & & & & \frac{N}{2} \end{pmatrix} \tag{I.80}$$

$$H_2 = \begin{pmatrix} u_0 & u_{-1} & \dots & u_{-N} & & & \\ u_1 & u_0 & u_{-1} & \ddots & \ddots & & \\ \vdots & u_1 & u_0 & \ddots & \ddots & \ddots & \\ u_N & \ddots & \ddots & \ddots & \ddots & \ddots & u_{-N} \\ & u_N & \ddots & \ddots & \ddots & \ddots & \vdots \\ & & \ddots & \ddots & \ddots & \ddots & u_{-1} \\ & & & u_N & \dots & u_{-1} & u_0 \end{pmatrix}. \tag{I.81}$$

The accuracy of finding the eigenvalues for this system is much higher than for the original equation (I.75), and the "fake" eigenvalues do not appear in the nonlinear spectrum.

I.3.5 Cauchy Integral

The problem of finding a discrete spectrum, as we have seen earlier, can be reduced to finding the zeros of the coefficient $a(\xi)$ in the upper complex half-plane. In this interpretation, the dependence of the coefficient a on the complex variable ξ can be understood as a function defined on the set of complex numbers. Therefore, we can apply the Cauchy integral formula to solve the above problem:

$$f(z_0) = \frac{1}{2\pi i} \int_\Gamma \frac{f(z)}{z - z_0} dz, \tag{I.82}$$

where D is a region in the complex plane with the boundary $\Gamma = \partial D$, $f(z)$ is a holomorphic function in $\bar{D}$, z_0 is a point in D. We consider one turn, i.e. one bypass along the border of the region D. To find the eigenvalues, we use the method described in [33, 34], which uses the set of contour integrals $\{s_p\}_{p=1}^{P}$:

$$s_p = \frac{1}{2\pi i} \int_\Gamma \xi^p \frac{a'(\xi)}{a(\xi)} d\xi = \sum_{j=1}^{P} \xi_j^p, \quad p = 1...P. \tag{I.83}$$

where P is the number of zeros of the coefficient $a(\xi)$ in the upper half-plane. Each contour integral gives us the sum to the right in the expression that is used to find all the eigenvalues (Fig. I.4). When $p = 0$, the expression gives the total number of zeros inside the contour Γ. This fact can be used to count the number of discrete eigenvalues for a given signal. To do this, we rewrite the formula (I.83) for a contour that passes along the real axe and closes in the upper half-plane through an infinitely distant point (Fig. I.5):

$$N = \frac{1}{2\pi} Arg(a(\xi))|_{-\infty}^{+\infty}, \tag{I.84}$$

where N is the total number of solitons in the signal, the spectral parameter ξ takes values from $-\infty$ to $+\infty$ on the real axe. In the framework of this task $N = P$. This formula is convenient for numerical calculation: choosing a sufficiently large interval of the real straight

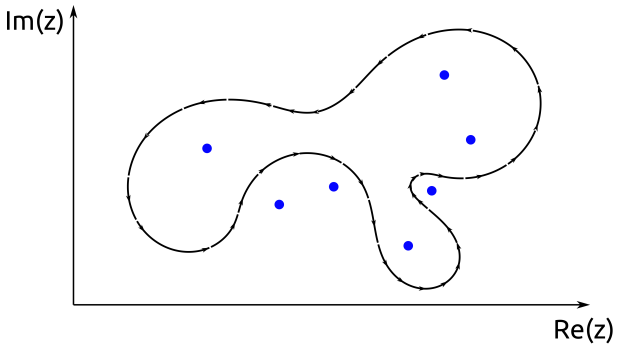

Figure I.4: Traversing several zeros on the complex plane.

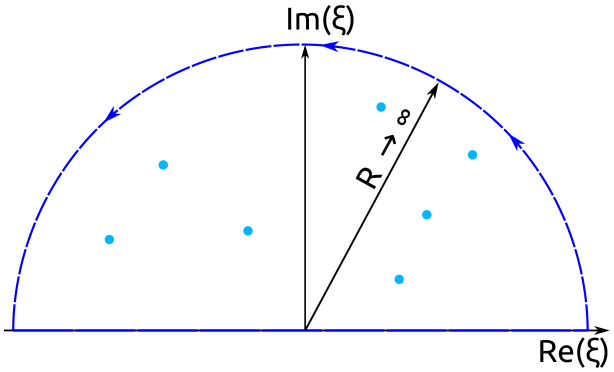

Figure I.5: Calculate the number of zeros of a complex function.

line and calculating the phase change of the coefficient $a(\xi)$, we will know exactly the number of discrete eigenvalues.

To find the individual eigenvalues, the so-called Newton identities $\{\sigma\}_{p=1}^{P}$ are used:

$$\begin{aligned} -\sum_{j=1}^{P}\xi_j &= \sigma_1, \\ \xi_1\xi_2 + \xi_2\xi_3 + ... + \xi_{P-1}\xi_P &= \sigma_2, \\ &... \\ (-1)^P\xi_1\xi_2...\xi_P &= \sigma_P. \end{aligned} \tag{I.85}$$

which are associated with the value of the integrals:

$$\begin{aligned} s_1 + \sigma_1 &= 0, \\ s_2 + s_1\sigma_1 + 2\sigma_2 &= 0, \\ &... \\ s_P + s_{P-1}\sigma_1 + ... + s_1\sigma_{P-1} + P\sigma_P &= 0 \end{aligned} \tag{I.86}$$

Solving this system, we obtain the values of each Newton identity, calculated by the recurrence formula:

$$\sigma_p = -\frac{1}{p}\left(s_p + \sum_{j=1}^{p-1} s_j\sigma_{p-j}\right), \quad p = 1...P. \tag{I.87}$$

As a result, σ_p (up to a sign) are Viète's formulas for the polynomial

$$M(z) = z^P + \sigma_1 z^{P-1} + \sigma_2 z^{P-2} + ... + \sigma_{P-1} z + \sigma_P, \tag{I.88}$$

which zeros coincide with the zeros of the original coefficient $a(\xi)$. Using any algorithm to find the zeros of a polynomial, we thus calculate the discrete spectrum $\{\xi_j\}_{j=1}^P$.

One of the ways to find the zeros of the polynomial I.88) is to go to the problem of finding eigenvalues of the so-called companion matrix $C(M)$:

$$C(M(z)) = \begin{bmatrix} 0 & 0 & \dots & 0 & -\sigma_P \\ 1 & 0 & \dots & 0 & -\sigma_{P-1} \\ 0 & 1 & \dots & 0 & -\sigma_{P-2} \\ \vdots & \vdots & \ddots & \vdots & \vdots \\ 0 & 0 & \dots & 1 & -\sigma_1 \end{bmatrix}, \tag{I.89}$$

for which the polynomial (I.88) is a characteristic polynomial. There exist effective algorithms of finding eigenvalues of such a matrix, for example, the QR-algorithm [35, 36, 37].

Part II

Study of soliton content in the standard optical signals

II.1 Methodology

The method of nonlinear Fourier transform allows us to examine the nonlinear component of the signals that were developed in the framework of the linear theory. The mathematical apparatus of the nonlinear Fourier transform allows a better understanding of the structure of the signals, as well as their features associated with nonlinear effects. Standard signals can (at a certain power level) contain coherent structures — solitons. Solitons can be represented as $q(t) = A\mathrm{sech}(At + \delta)e^{2i\omega t + i\theta}$ and are of interest from an applied point of view, since they contain four variable parameters in which information can be encoded: soliton amplitude A, time shift δ, soliton complex frequency ω and phase shift θ.

The fact of the presence of solitons in a signal can be detected using the direct Zakharov-Shabat problem. The spectrum of the operator L in the problem (I.5), where the function $q(t, z)$ is the signal to study, can give a representation of the structure of this signal. If there are discrete values in the spectrum, then there are also solitons. This feature will be used for further analysis of standard optical signals, and the number of solitons is determined by the formula (I.84). By standard signals, we mean WDM and OFDM systems, which are now widely used for optical communication. For the futher analysis of signals, we use numerical algorithms, which are described in Chapter I and previously tested on test signals: a rectangular pulse and a Satsuma-Yajima signal.

The signal parameters at which solitons can exist depend on the system. For further study, we consider two parameters inherent in each signal. They are the L_1 and L_2 norms, calculated as follows:

$$L_1(q) = \|q(t, z)\|_{L_1} = \int_{-\infty}^{+\infty} |q(t, z)|dt, \tag{II.1}$$

$$L_2(q) = \|q(t,z)\|_{L_2} = \int_{-\infty}^{+\infty} |q(t,z)|^2 dt, \tag{II.2}$$

where $q(t,z)$ is signal to study, t and z — time and space coordinates.

Two standard methods of telecommunication signal multiplexing were chosen for the study: OFDM — orthogonal frequency-division multiplexing and WDM — wavelength-division multiplexing. Without loss of generality, we focus on two modulation formats: phase shift keying (PSK) and quadrature amplitude modulation (QAM).

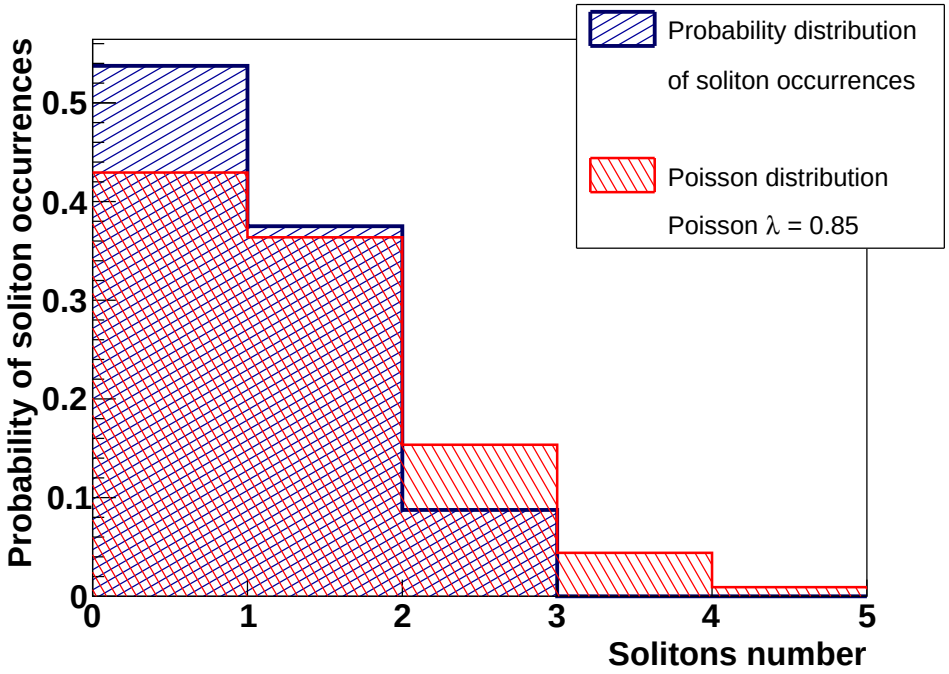

Figure II.1: The probability of soliton occurrence in an OFDM signal with QPSK modulation, 128 subcarriers and an average power of -18 dBm.

In general, signals can contain more than one soliton. In this case, if the average power of the signal is at the threshold of the existence of solitons, then signals that do not contain or contain one or more solitons can appear in the set of signals with random data. When we collect statistics on such signals, we obtain the probability distribution of the existence of solitons in the signal, presented in Fig. II.1. The figure also shows the Poisson distribution ($P(x;\lambda) = e^{-\lambda} \cdot \lambda^N / N!$) with the value $\lambda = 0.85$, obtained by fitting the experimental distribution. The number of events in the theoretical distribution is 10^6, and 160 in the experimental one. Figure II.2 illustrates the case when solitons always exist in the signal for given parameters, but their number changes depending on the initial data. In this case, the distribution is well described by the Gaussian distribution $G(x) = \frac{1}{\sigma\sqrt{2\pi}} e^{-\frac{(x-\mu)^2}{2\sigma^2}}$ with a mathematical expectation μ and standard deviation σ.

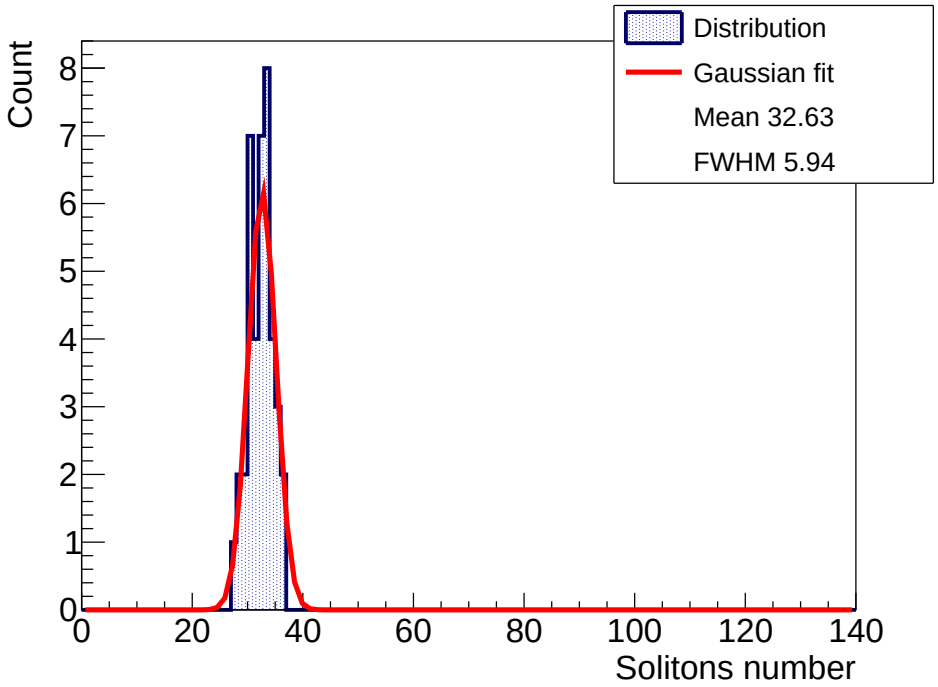

Figure II.2: The distribution of the number of solitons in OFDM signals with 16-QAM modulation, 64 subcarriers and an average power of -11 dBm.

Previously, these types of signals were not studied for the content of solitons; therefore, at the first stage, we consider only the fact of the existence of solitons, and not their number and characteristics. It is important to note that in this part of the work we are interested in the fact of the presence of solitons in the signal, and not in their number, therefore the probability of the existence of a discrete spectrum is calculated as the ratio of the number of signals in which at least one soliton is present to the total number of signals with given parameters.

The average power of the signal (P_{ave}) is related to L_2 norm (I.36) as $P_{ave} = L_2/T$, where T is the symbol interval (the length of one symbol). In this work, we use mW and dBm as the units of power measurement, which is calculated as P dBm $= 10\log_{10}(P\ [\text{mW}])$. For numerical simulation, we used the following optical fiber parameters: the group velocity dispersion $\beta_2 = -21.5$ ps^{2}km^{-1} and the Kerr nonlinearity coefficient $\gamma = 1.27$ W^{-1}km^{-1}.

To determine the intervals in which optical signals will be studied, we turn to the criterion for the existence of solitons (I.43), which is written in dimensional units as

$$P_{ave} > \frac{|\beta_2|\pi^2}{4\gamma T_s^2}, \tag{II.3}$$

where T_s is the time interval under study, which in this work is equal to the duration of one symbol for an OFDM or WDM signal. Figure II.3 shows the dependence of the minimum average signal power, above which a discrete spectrum may exist, on the symbol duration. The green lines indicate the duration of the symbols studied in this work. For 10 ns, the

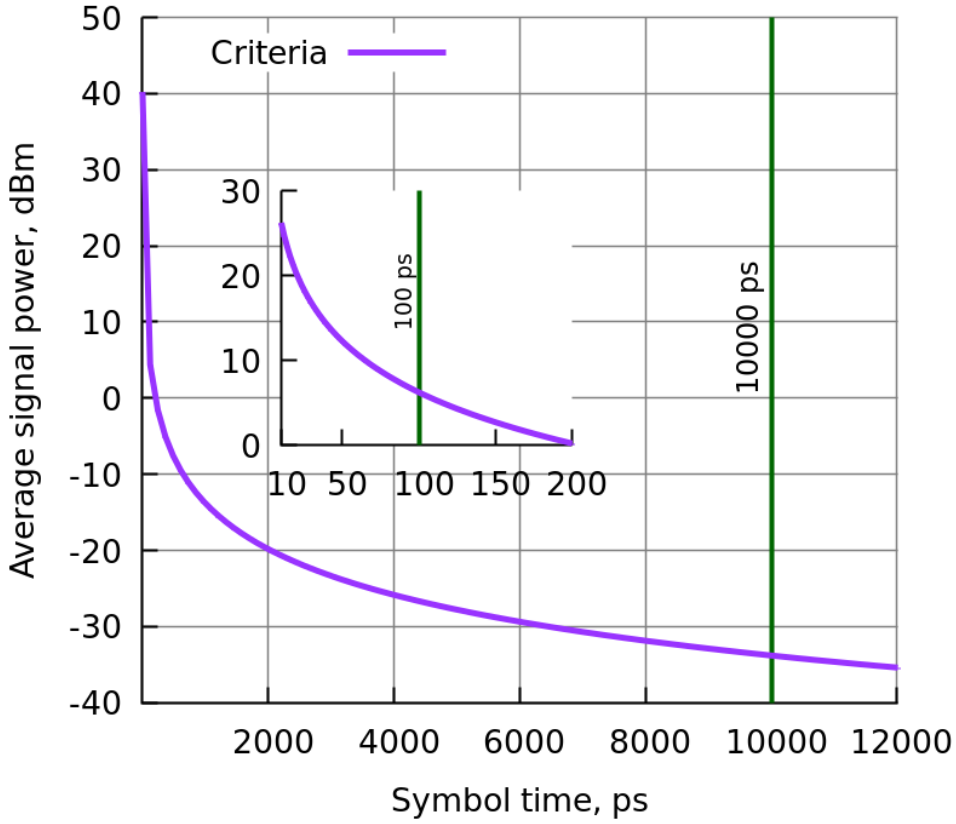

Figure II.3: The dependence of the criteria II.3 in dimensional units on the symbol duration T.

threshold is below -30 dBm (-33.8 dBm), while for 100 ps the threshold is much larger (6.2 dBm). Based on these values, we select the necessary power levels for the study of each type of signal. It should be noted that the graph shows the total average signal power, but for WDM systems the average power per channel is more often used. This is further taken into account when recalculating.

II.1.1 Modulation

In the work we use quadrature amplitude modulation (QAM), which provides significant improvements for data transmission. For higher modulation orders, high speeds are achieved, but the noise level requirement also increases. The main parameters of the systems, depending on the constellation diagram, are presented in Table II.1. Although the first three types of

Table II.1: QAM formats and bit rate comparison

Modulation type	Bits per symbol	Symbol rate
BPSK	1	1 × bit rate
QPSK	2	1/2 × bit rate
8PSK	3	1/3 × bit rate
16QAM	4	1/4 × bit rate
32QAM	5	1/5 × bit rate
64QAM	6	1/6 × bit rate

modulation in the Table are called phase-shift keying (PSK), they can be represented via QAM modulation. Examples of constellation diagrams used in the work are presented in Fig. II.4.

II.1.2 Measurement of the signal transmission quality

The main values for assessing the quality of signal transmission in the optical system are two parameters: EVM — error vector magnitude and BER — bit error ratio. EVM is determined by the formula

$$\mathrm{EVM}_m = \frac{\sigma_{\mathrm{err}}}{|E_{t,m}|},\ \sigma^2_{\mathrm{err}} = \frac{1}{I}\sum_{i=1}^{I}|E_{\mathrm{err},i}|^2,\ E_{\mathrm{err},i} = E_{r,i} - E_{t,i}. \tag{II.4}$$

where the propagated vector E_r deviates by the vector E_{err} from the ideally transmitted vector E_t, and BER is connected with EVM as

$$\mathrm{BER} \approx \frac{(1-L^{-1})}{\log_2 L}\mathrm{erfc}\left[\sqrt{\frac{3\log_2 L}{(L^2-1)}\frac{1}{(k\mathrm{EVM}_m)^2\log_2 M}}\right]. \tag{II.5}$$

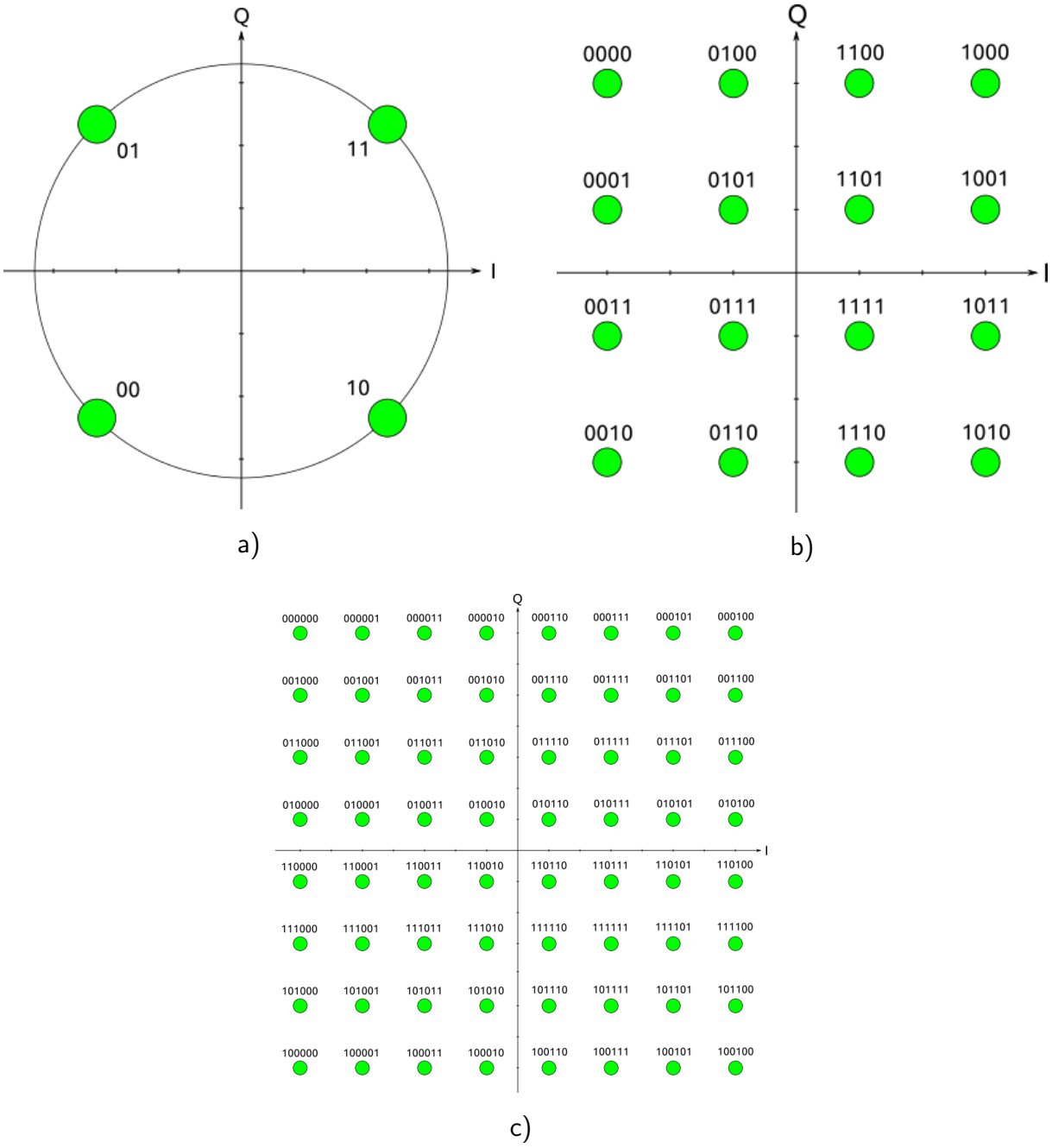

Figure II.4: Constellation diagrams for (a) QPSK, (b) 16-QAM and (c) 64-QAM.

In the formula L is the number of signal levels that are identical in each dimension of the constellation, $\log_2 M$ is the number of bits encoded in each QAM symbol. More information about these parameters can be found in [38].

Q^2-factor is connected to EVM as $Q^2 = 1/\mathrm{EVM}^2$. We will use this definition in the future to assess the quality of the transmission system. The maximum of Q^2 factor corresponds to the most optimal transmission parameters.

II.2 OFDM signal

II.2.1 Signal generation

The OFDM signal combines modulation and multiplexing. To form a symbol, the term "subcarrier" is used, which in fact is one of the Fourier harmonics in the frequency space from which the signal is formed. One isolated symbol on a time slot of T is the sum of independent subcarriers modulated according to the chosen modulation type:

$$s(t) = \sum_{k=0}^{N-1} X_k e^{i2\pi kt/T}, \tag{II.6}$$

where N — number of subcarriers, T — symbol duration, X_k — digital data. An OFDM signal consists of a sequence of such symbols separated by a guard interval T_g, which in this case we do not use. Depending on the modulation type, the corresponding constellation diagram is selected (Fig. II.4).

In practice, the number of subcarriers is chosen as $N = 2^p$ (p is a positive integer) in order to use the Fast Fourier Transform (FFT) algorithms. The scheme of forming the OFDM signal is shown in Fig. II.5. The input is serial data which is divided into N parallel threads. Each data stream is encoded according to the selected modulation format (QPSK or QAM). Each individual stream corresponds to a specific frequency, and the encoded data determines the complex amplitude for that frequency. Thus obtained N numbers are used further in the FFT, the result of which is the one OFDM symbol. The sequence of such symbols forms a complete OFDM signal, which is used to transmit information. To decode a signal, the procedure is performed in the reverse order: the inverse FFT is performed, the data is decoded and their order is restored.

II.2.2 Results

In dimensional units, we examined OFDM symbols with 10 ns duration and QPSK, 16-, 64-, and 1024-QAM modulation types. The number of subcarriers varies from 16 to 1024 with a full FFT size of 1024. First of all, we checked whether the number of solitons in the signal

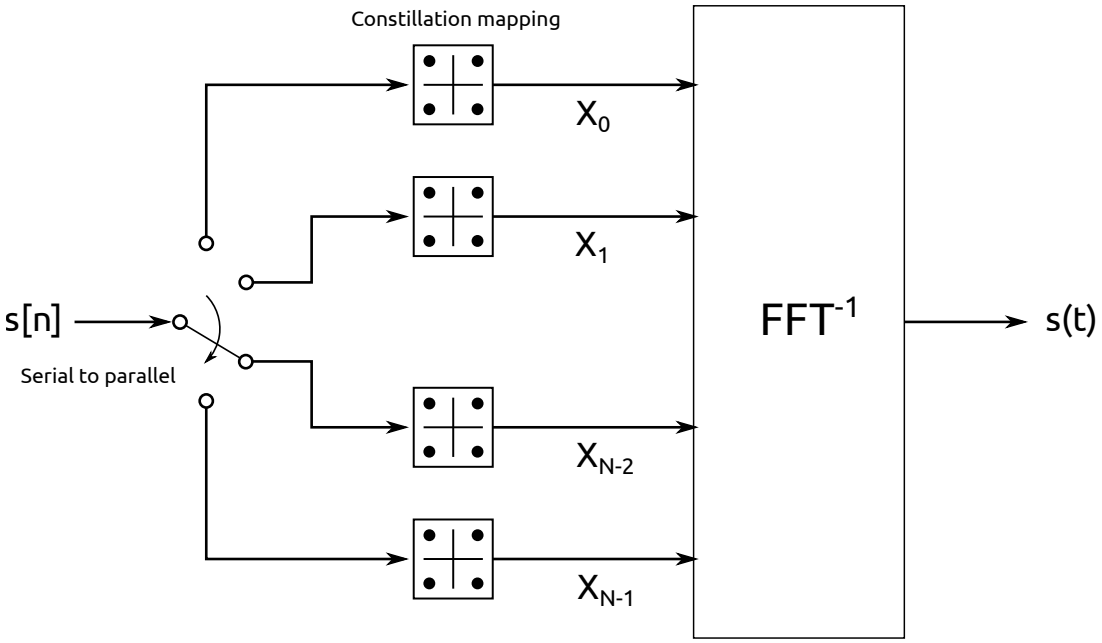

Figure II.5: OFDM signal generation

changes with a varying FFT size. We observe the number of solitons does not change with the increase of the FFT size, since the size of the FFT is equal to 128.

Next, we collect statistics on 200 simulated symbols with random input data with fixed parameters for each point in the graphs. We used the Mersenne Twister pseudo-random generator of 32-bit numbers with a state size of 19937 bits (mt19937). Figure II.6 shows how the probability of a soliton content in a signal changes depending on the L_1 norm for a signal with 128 subcarriers and QPSK and 16-QAM modulation. The first level L_1 of the norm, calculated by the formula (I.33) and equal to 1.57, lies to the left outside the graph. Afterward in the paper, we focused on the study of the dependence of the probability of the existence of solitons in a signal on the value of the average signal power. This is due to the fact that this characteristic has a physical equivalent and can be experimentally calculated in an experiment.

Figure II.7 (a) presents the results of the dependence of the probability of the existence of solitons in OFDM signals with 16-QAM on the average signal power. As the number of subcarriers increases, the power necessary for the existence of solitons increases. This effect can be explained in Figure II.7 (b), which shows a similar graph, taking into account the fact that the average power is divided into each "channel" which is the corresponding subcarrier. The graph shows that in reality the probability of existence is determined by the power density of each channel, which does not depend on the total number of subcarriers. As a result, with an increase in the number of subcarriers, the total signal power required for the existence of solitons also increases. A similar effect is observed for other types of modulation (Fig. II.8). From the obtained results it can be concluded that the average power band per channel is in

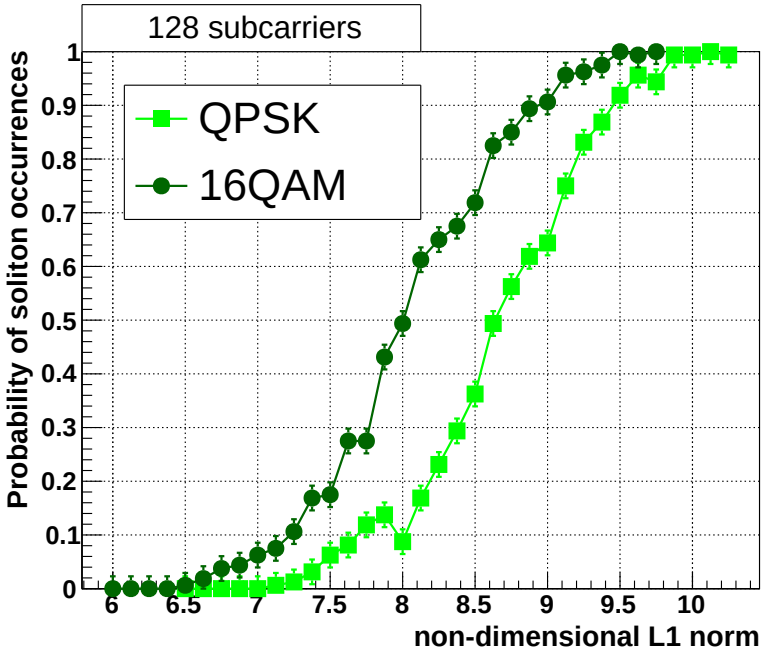

Figure II.6: Dependence of the probability of soliton occurrence in OFDM signals with 128 subcarriers and QPSK and 16-QAM modulation.

the range from -42 dBm to -37 dBm. Based on this data, we can predict the existence limits of solitons for other signals.

However, the type of modulation also affects the probability distribution. Figure II.9 demonstrates that with an increase in the order of the constellation diagram, and hence with an increase in the number of bits of information encoded in one symbol, the required average signal power for the existence of solitons decreases. This fact is well seen when comparing QPSK and other types of modulation. Irrespective of the number of subcarriers, there is a tendency that for QPSK modulation, the average signal power is higher than for others. If we proceed to the dependence on the average power per channel, the situation will not change (Fig. II.10).

As expected, for a complex signal the level of L_1 and L_2 norms (and hence P_{ave}), at which solitons exist in the signal, is higher than for a simple rectangular signal. This is consistent with the criteria (II.3), which can also be used for preliminary analysis in other existing systems.

At the next stage, it is necessary to compare the obtained power levels with the levels optimal for transmission. Figure II.11 (b) shows the Q^2-factor for an OFDM signal with 16-QAM, 128 subcarriers and a duration of 10 ns from the average signal power. The system parameters were previously defined in the section II.1. The maximum Q^2-factor in such a system reaches at power levels of -15 — -14 dBm. In Figure II.11 (a) it can be seen that at such power levels solitons exist in all signals.

In the general case, solitons and dispersion waves propagate through the fiber in different

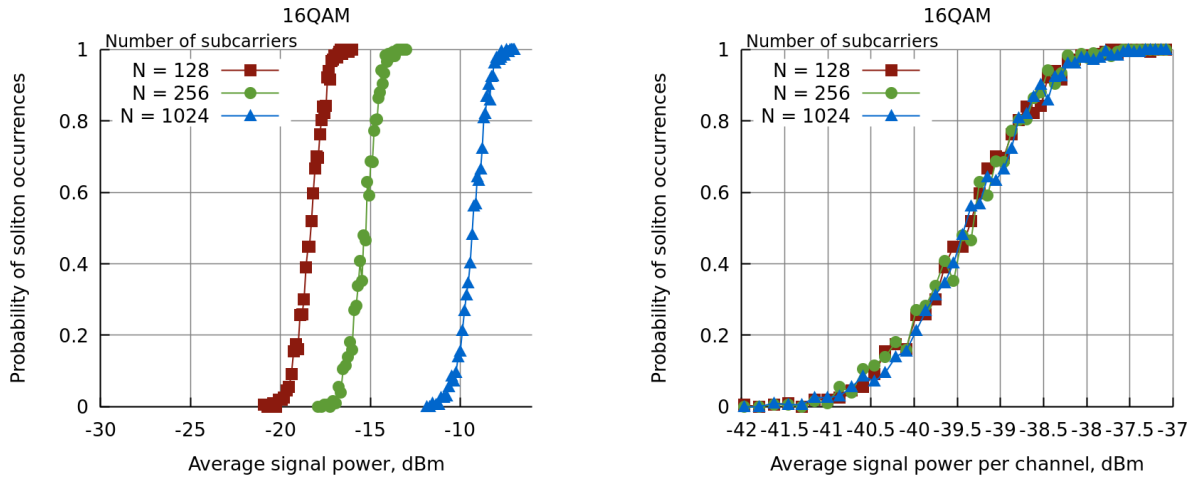

a) b)

Figure II.7: The dependence of the probability of soliton occurrence for OFDM signals with 16-QAM and a symbol duration of 10 ns from (a) on average signal power, (b) on average signal power per channel.

ways. The most important difference is that the dispersion for solitons is balanced by nonlinear effects. The existence of solitons in a standard OFDM signal has the potential to make some contribution in propagation. Understanding of this fact may affect coding and modulation of signals in optical communication, as it can lead to an improvement in the efficiency of optical communication lines. However, in practice, the appearance of solitons does not have a large effect on the propagation dynamics of the OFDM signal at the considered power levels. At higher levels, it is already possible to observe the evolution of individual solitons in a common signal, however, these events are rare, and more research is needed to determine the parameters and degree of influence of solitons on the signal.

II.3 WDM signal

II.3.1 Signal generation

The wavelength-division multiplexing (WDM) technology allows to simultaneously transmit several information channels over a single optical fiber at different frequencies. It uses existing communication lines and allows you to organize two-way transmission. The principle of WDM is based on the fact that information can be transmitted simultaneously at several wavelengths in a single fiber-optic channel. Each individual wavelength is called a "channel" , and then we follow this terminology.

One isolated WDM symbol is formed as a sum of carrier functions modulated according

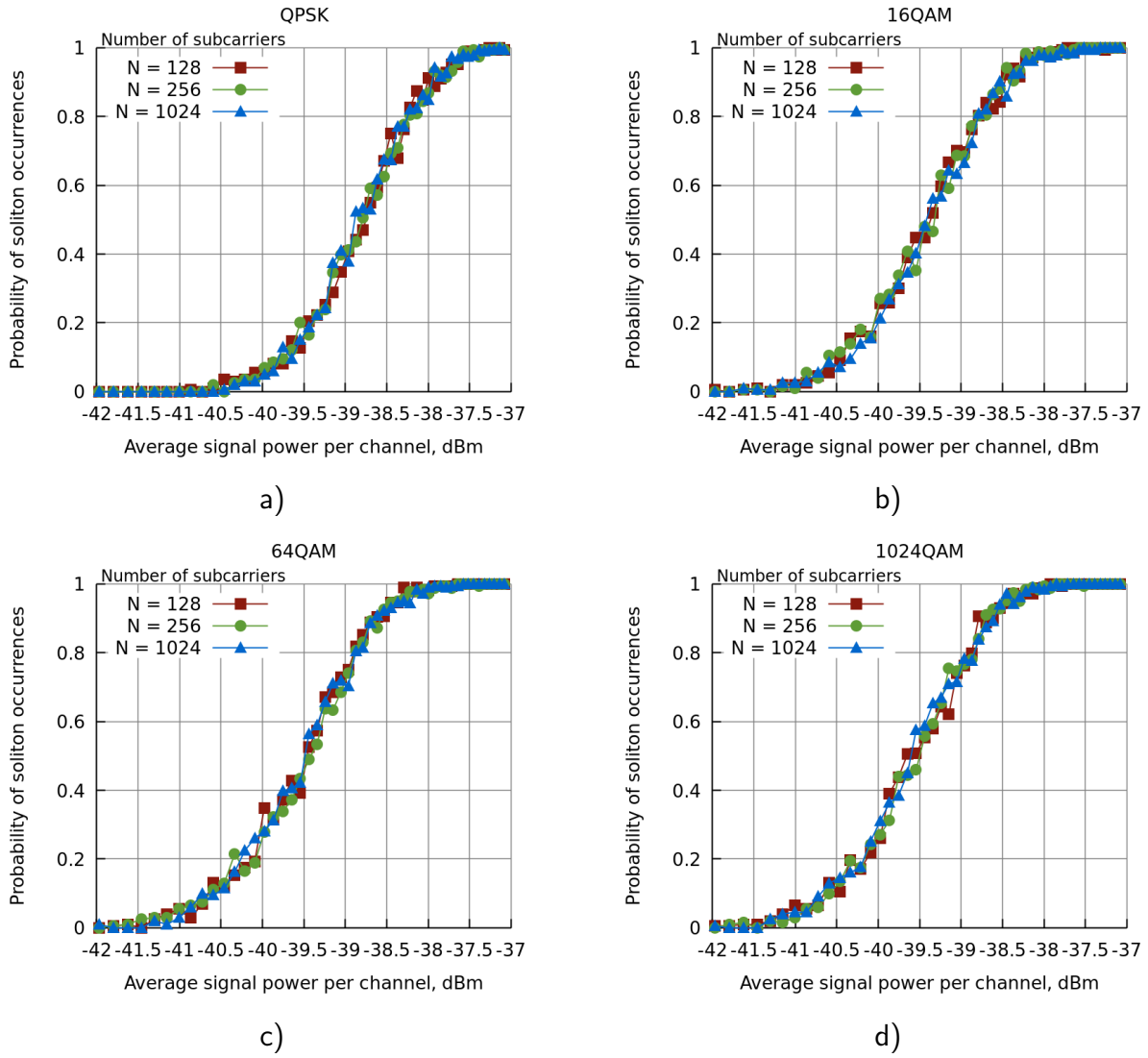

Figure II.8: The dependence of the probability of soliton occurrence in the OFDM symbol with a duration of 10 ns and (a) QPSK, (b) 16-QAM, (c) 64-QAM, (d) 1024-QAM modulation on the average signal power per channel.

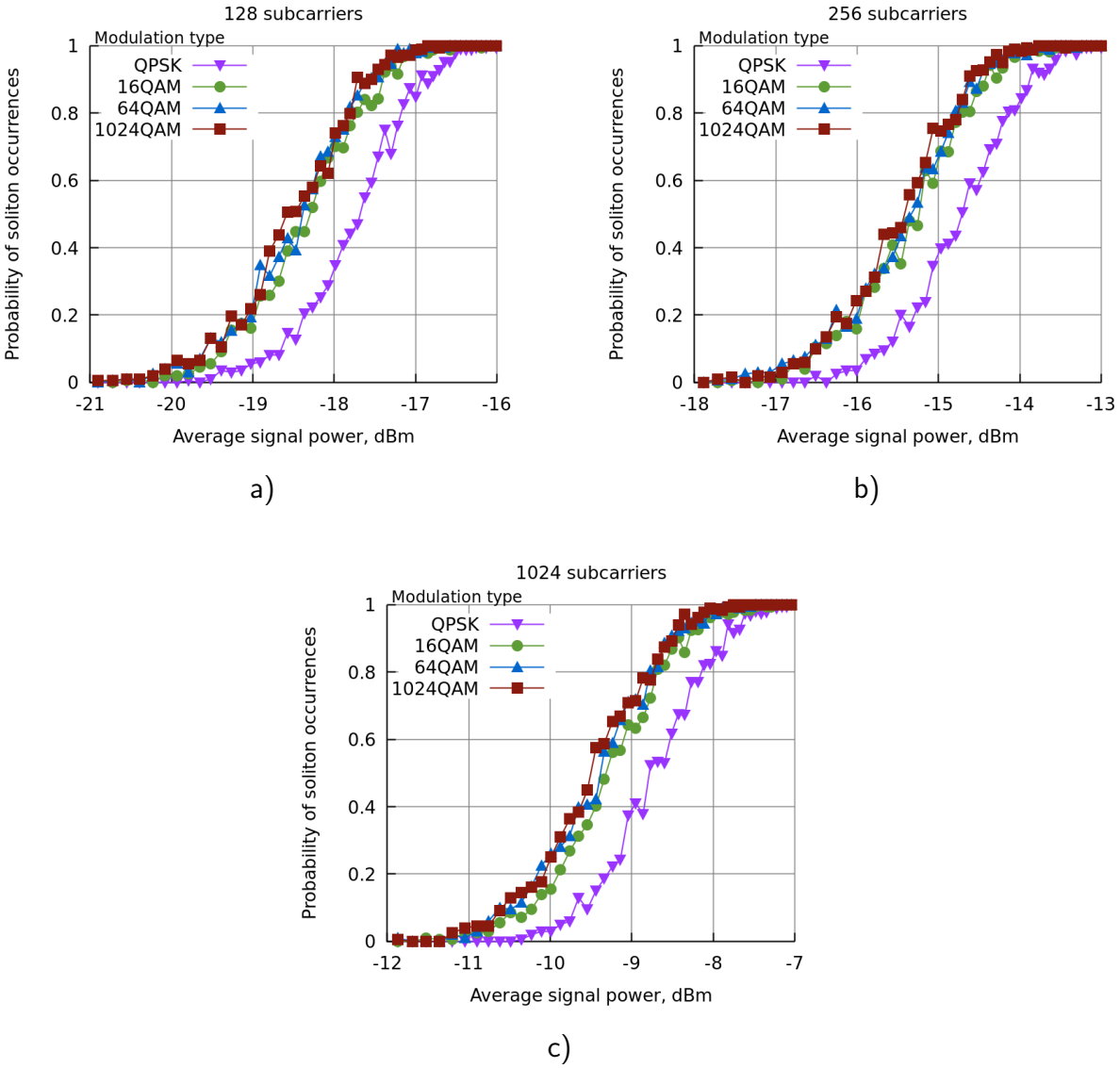

Figure II.9: The dependence of the probability of soliton occurrence in the OFDM symbol with a duration of 10 ns and (a) 128, (b) 256, (c) 1024 subcarriers on the average signal power.

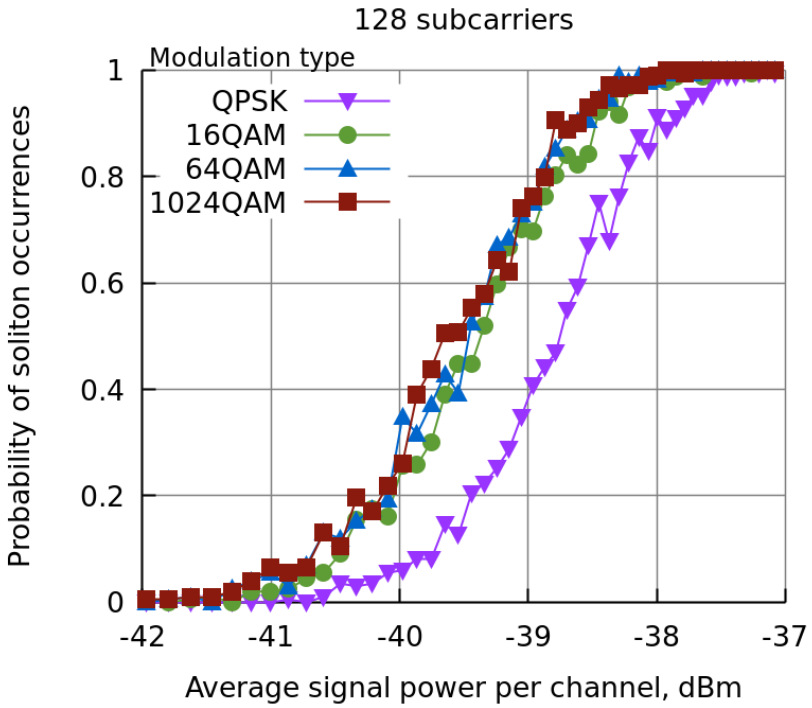

Figure II.10: The dependence of the probability of soliton occurrence in the OFDM symbol with a duration of 10 ns and 128 subcarriers on the average signal power per channel.

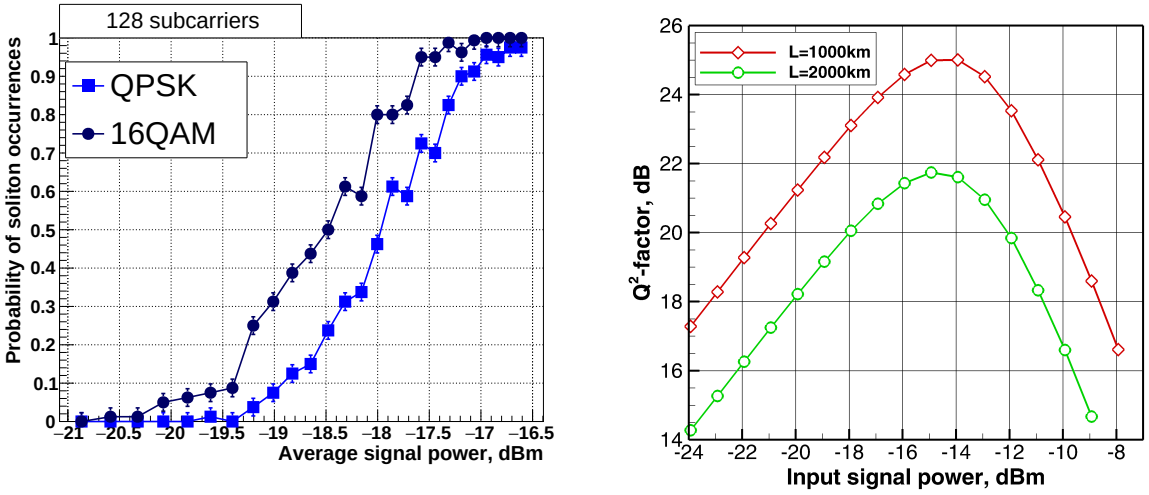

a) b)

Figure II.11: (a) The dependence of the probability of soliton occurrence, (b) the dependence of the Q^2-factor for an OFDM signal with 128 subcarriers and 16-QAM on the average signal power.

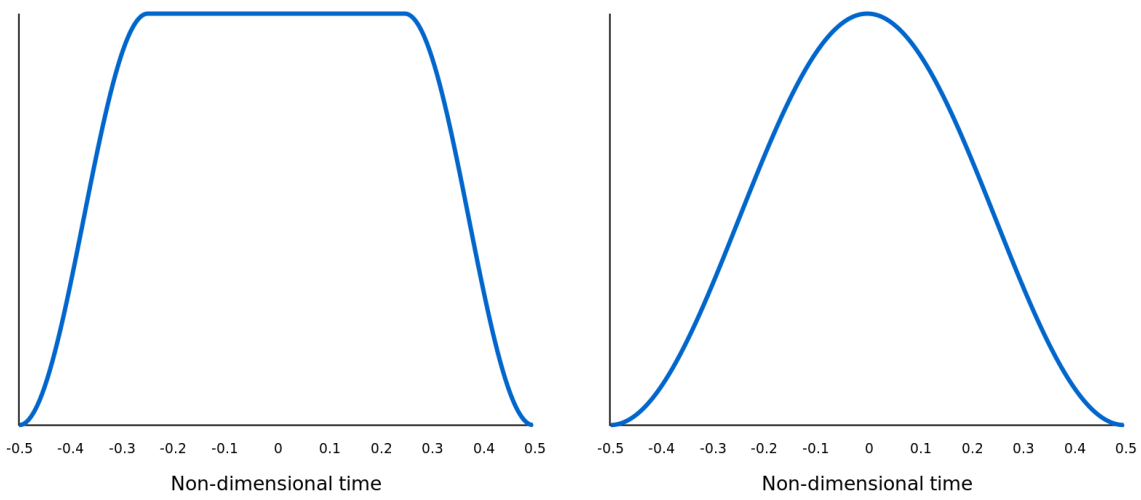

Figure II.12: Examples of carrier functions for WDM signal

to their carrier frequency and encoded data:

$$s(t) = \sum_{n=-N/2}^{N/2} e^{i\omega_n t} C_n f(t), \tag{II.7}$$

N — number of channels, ω_n — carrier frequency, C_n — digital data (corresponding to the constellation diagram), $f(t)$ — carrier function.

Without loss of generality, we consider the following return-to-zero (RZ) carrier function (Fig. II.12 (a)):

$$f(t) = \begin{cases} \frac{1}{2}\left[1 - \cos\left(\frac{4\pi t}{T}\right)\right], & 0 \le t \le \frac{T}{4} \text{ or } \frac{3T}{4} \le t \le T \\ 1, & \frac{T}{4} < t < \frac{3T}{4} \end{cases} \tag{II.8}$$

As a carrier function, one can also use other RZ functions, for example

$$f(t) = \frac{1}{2}\left[1 - \cos\left(\frac{2\pi t}{T}\right)\right], \quad 0 \le t \le T, \tag{II.9}$$

represented in Fig. II.12 (b). Also used is the widespread communication function "raised-cosine filter" . In time space, it is expressed as follows:

$$f(t) = \begin{cases} \frac{\pi}{4T}\ \mathrm{sinc}\left(\frac{1}{2\beta}\right), & t = \pm\frac{T}{2\beta} \\ \frac{1}{T}\ \mathrm{sinc}\left(\frac{t}{T}\right)\frac{\cos\left(\frac{\pi\beta t}{T}\right)}{1-(\frac{2\beta t}{T})^2}, & \text{otherwise} \end{cases} \tag{II.10}$$

However, we will focus on the study of signals with a carrier function in the form (II.10), while other formats are left for future work.

The data is encoded according to the chosen modulation format, and the carrier frequency ω_n is calculated by the formula

$$\omega_n = \Delta\omega \cdot n, \quad n = -N/2 ... N/2, \tag{II.11}$$

where $\Delta\omega$ is the inter-channel distance equal in this work to 25 GHz. The duration of one symbol is 100 ps.

II.3.2 Results

At this stage of the work, we study WDM symbols with QPSK, 16-, 64-, 1024-QAM and vary the number of channels from 9 to 51. Similar to OFDM signals, we collected statistics on 200 WDM symbols for each parameter set. The dependence of the probability of existence of solitons in a signal on the average signal power per channel for different types of modulation and different number of channels is shown in Fig. II.13. We want to emphasize that, unlike the OFDM signal, the graphs show the average power per WDM channel.

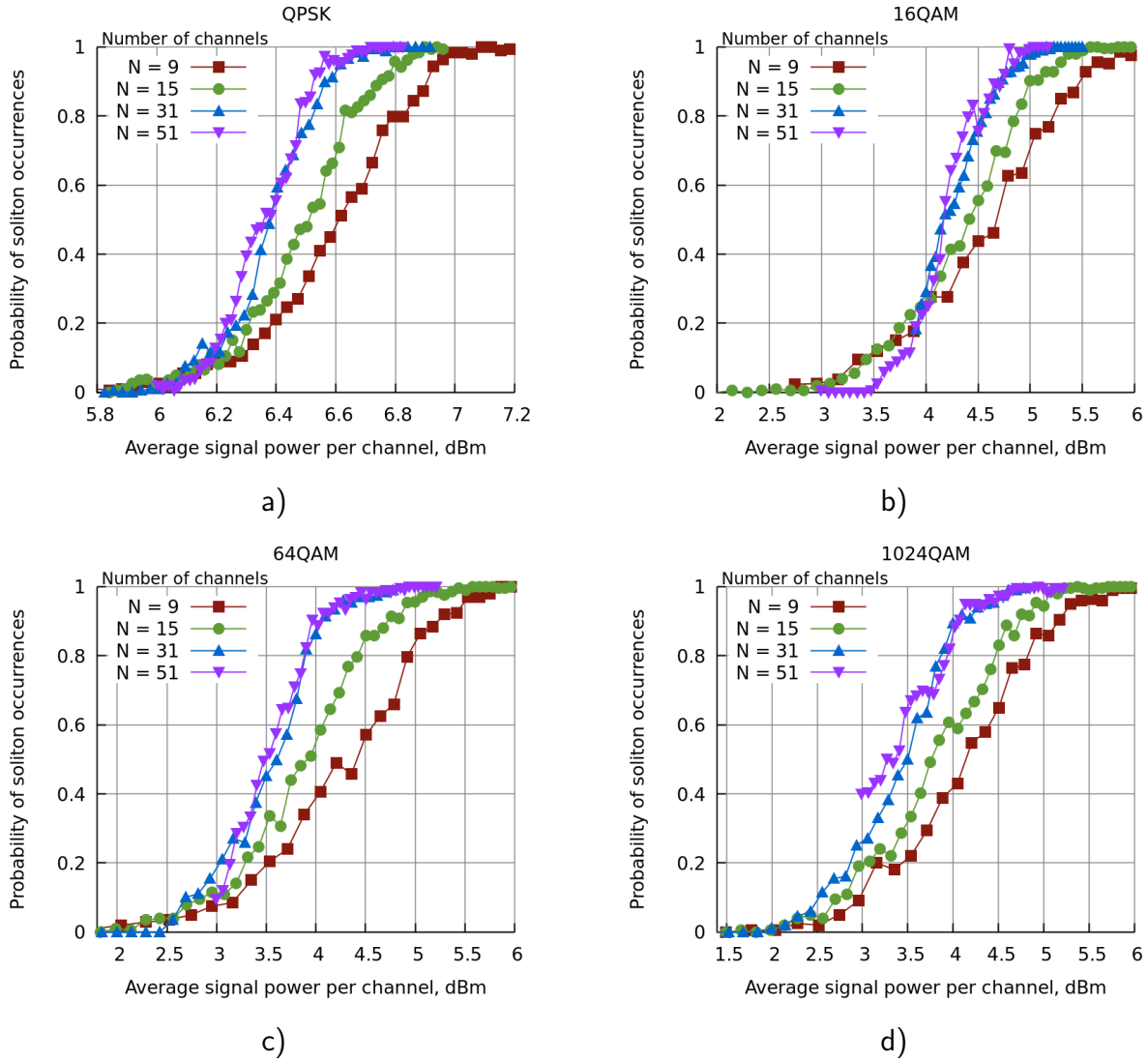

Figure II.13: The dependence of the probability of solitons occurrence in a WDM signal on the average signal power per channel with a duration of 100 ps and (a) QPSK, (b) 16-QAM, (c) 64-QAM, (d) 1024-QAM modulation.

Comparing the graph in Fig. II.13 (a) with others, it can be noted that for QPSK modulation the power level is much higher than for other types of modulation, and it is situated in a narrow range from 5.8 dBm to 7 dBm. For 16-, 64-, 1024-QAM, the band is from 2 dBm to 6 dBm. With an increase in the number of channels, the threshold power decreases, and the power difference for a different number of channels is retained for all types of modulation. For a WDM signal, we observe the same effect as for OFDM signals: with an increase in the modulation order, the threshold power decreases (Fig. II.14). In addition, WDM signals with QPSK modulation have a soliton threshold power much more than with other types of modulation. Also, for WDM signals, the difference between 16-, 64-, and 1024-QAM modulations is more significant than in OFDM signals. For example, by increasing the number of channels, we can split 16-QAM and 64-QAM for 51 channels (Fig. II.14 (d))

These features demonstrate that, despite the similar signal generation processes, WDM and OFDM systems have a different internal structure, and also depend on the selected parameters in different ways.

To estimate the power levels that are optimal for signal propagation, we calculated the dependence of the Q^2-factor on the power per channel presented in Fig. II.15. The optimal transmission level is -14 dBm. It is in the power range where solitons do not exist. This represents a fundamental difference from the OFDM signal, for which the optimal power level corresponded to the signals containing the soliton component.

The fact that solitons do not exist in this range is also of interest in the framework of the nonlinear data transfer theory. If there are no solitons, then Ω_{sol} (I.18) is missing in the formula for computing the kernel of the Zakharov-Shabat problem (I.7). It means that the remaining member (I.19), which is a simple Fourier transform, completely defines the kernel. In such a case, existing algorithms can be simplified, and there is no need to calculate the complete nonlinear spectrum to implement a nonlinear Fourier transform. This property can be used to improve transmission over optical links.

In another case, with an increase in transmission power, the results obtained can help assess the conditions when solitons will exist in a WDM system. In these solitons, useful information can be encoded, or they can be used as special triggers of signal system malfunctions.

The results obtained for WDM and OFDM systems show that coherent structures are an integral part of these systems, and therefore should be study along with other effects. The results are interesting because the features associated with nonlinearity can be evaluated and used in practice. For OFDM signals, the power levels that are optimal for propagation, under certain configurations, coincide with the mode when solitons exist in the signals. For WDM signals, existing systems use modes when there are no solitons, which can also be used to refine and improve existing models.

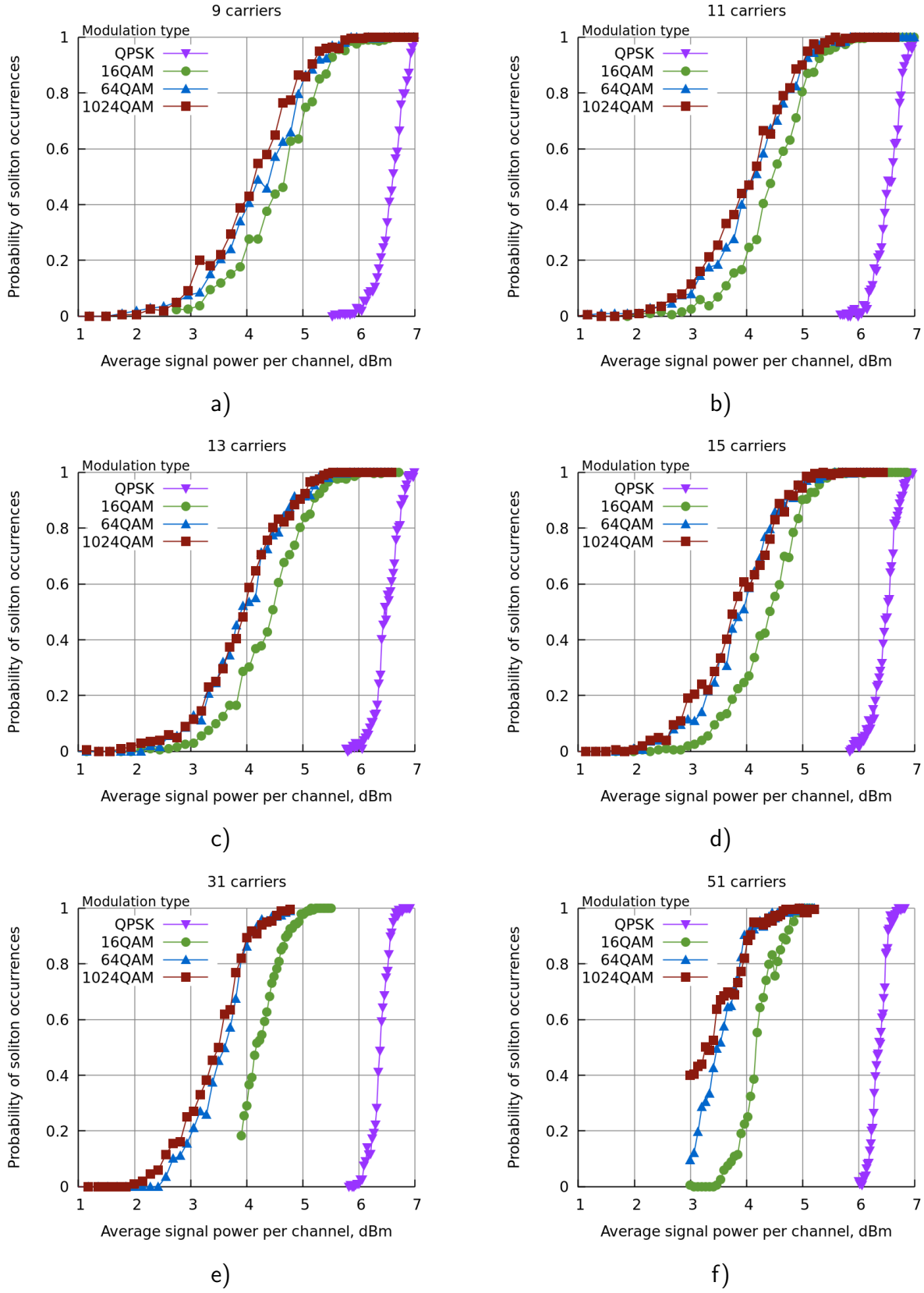

Figure II.14: The dependence of the probability of soliton occurrence in a WDM signal with (a) 9, (b) 11, (c) 13, (d) 15, (e) 31 and (f) 51 channels.

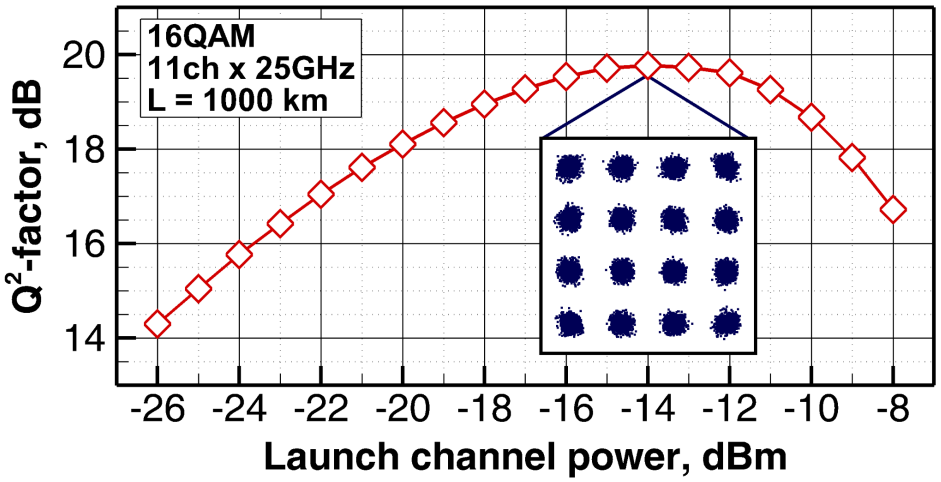

Figure II.15: The dependence of the Q^2-factor on the WDM signal power with a duration of 100 ps and an inter-channel distance of 25 GHz.

Conclusion

One of the goals of this work was to show that the existing linear systems are in fact nonlinear, and to overcome the fundamental barrier of the linear paradigm of data transfer. Nonlinear effects carry the potential to increase the capacity of existing systems. This work is one of the first steps in the study of nonlinear Fourier transform, as a new foundation for future fiber-optic communication systems. Future fiber optic communication systems based on NFT are expected to exceed the throughput limits of existing WDM systems. The results obtained demonstrate that even now standard optical signals produce purely nonlinear effects that are not taken into account in the framework of the linear theory.

In the future, we will also need to understand how optical signals can be modulated and demodulated according to a new paradigm, and how physical constraints (for example, bandwidth or power limitation) can be taken into account and represented in the signal space (in the nonlinear spectrum) to move from the mathematical background to the actual implementation of the system. To avoid potential problems due to digital processing, one can think of schemes for fully optical processing (similar to the optical implementation of the Fourier transform for all-optical OFDM) or schemes for multiplexing and demultiplexing signals in the nonlinear spectrum (by analogy with OTDM — Optical Time Division Multiplexing approaches and WDM).

Another important point is the understanding and modeling of the behavior of the entire transmission system. Since some propagation effects and systemic disturbances cannot be taken into account within the framework of integrable equations (attenuation, PMD, laser phase noise), an accurate analytical model of the system is not available. In addition, it is unclear how the linear noise from optical amplifiers affects the signal in the region of the nonlinear spectrum. Therefore, we need to implement an accurate numerical simulator that can be used to: check the system behavior and study its deviations from the analytical model, determine the statistical characteristics of the channel, estimate the achievable information transfer rates, optimize modulation and coding.

The model will also allow us to explore the transmission potential at large nonlinear and dispersive lengths, where NFT systems will allow the use of new parameter modes that are not achievable with conventional linear transmission schemes even when using nonlinear com-

pensation.

The potential of the nonlinear Fourier transform is huge. It is expected that the results of the development of NFT algorithms will have an impact that goes beyond the basic method of their application. Fast numerical algorithms and related mathematical methods, being very versatile, can find many interdisciplinary applications, for example:

- in photonics for the synthesis of fiber gratings [39], for the development of advanced fiber-laser devices [40] and to characterize extreme events in the form of the formation of killer waves [41];
- in hydrodynamics for nonlinear analysis of ocean waves [42];
- in geophysics for the analysis of seismological effects [43, 44]

and many others similar to the linear Fourier transform.

The obtained results were presented at student scientific conferences, and work [45] was published.

During my internship I could contribute to a optical communication theory. On my side, this internship noticeably broadened the list of my competences and allowed me to:

- learn how optical communication systems work and how a signal is transmitted,
- deepen my knowledge of quantum optics,
- improve my programming and data analysis skills,
- gain an experience of working in a group of international professionals.

I appreciated the variability of work in an optical laboratory and, consequently, the variety of required knowledge and competences.

But the most I enjoyed working in a group of professional researchers who love and respecttheir work. I found extremely motivating the friendly atmosphere between them; these are people who would gladly explain if there is something unclear and help if there is something difficult. To sum up, I would like to say that working at Nonlinear Photonics Laboratory gave me only positive experience and allowed me to grow as an independent researcher. I, in return, did all my best to bring maximum impact in the work of the laboratory. Having all this said, I consider this internship a partnership, beneficial for both sides.

Bibliography

[1] R. Essiambre and R. W. Tkach. Capacity trends and limits of optical communication networks. *Proceedings of the IEEE*, 100(5):1035–1055, May 2012.

[2] M. Cvijetic and I. Djordjevic. *Advanced Optical Communication Systems and Networks*. Artech House applied photonics series. Artech House, 2013.

[3] A. Hasegawa and T. Nyu. Eigenvalue communication. *Journal of Lightwave Technology*, 11(3):395–399, 1993.

[4] V. E. Zakharov and A. B. Shabat. Exact theory of two-dimensional self-focusing and one-dimensional self-modulation of waves in nonlinear media. *Soviet Physics JETP*, 34(1):62, 1972.

[5] A. Hasegawa and F. Tappert. Transmission of stationary nonlinear optical pulses in dispersive dielectric fibers. i. anomalous dispersion. *Appl. Phys. Lett.*, 23, 1973.

[6] L. F. Mollenauer, R. H. Stolen, and J. P. Gordon. Properties of optical soliton in a three level medium with quintic nonlinearity. *Phys. Rev. Lett.*, 45(13):1095, 1980.

[7] A. Hasegawa and Y. Kodama. Signal transmission by optical solitons in monomode fiber. *Proceedings of the IEEE*, 69(9):1145–1150, 1981.

[8] N. J. Doran and K. J. Blow. Solitons in optical communications. *IEEE Journal of Quantum Electronics*, 19(12):1883–1888, 1983.

[9] E. Rutherford. Lxxix. the scattering of α and β particles by matter and the structure of the atom. *The London, Edinburgh, and Dublin Philosophical Magazine and Journal of Science*, 21(125):669–688, 1911.

[10] C. S. Gardner, J. M. Greene, M. D. Kruskal, and R. M. Miura. Method for solving the korteweg-devries equation. *Physical review letters*, 19:1095–1097, 1967.

[11] Govind P Agrawal. *The Nonlinear Fiber Optics*. Academic press, 4th edition, 2007.

[12] P Lax. Integrals of nonlinear equations of evolution and solitary waves. *Comm. Pure Applied Math.*, pages 467–490, 1968.

[13] I. M. Gel'fand and B. M. Levitan. On the determination of adifferential equation from its spectral function. *Izv. Akad. NaukSSSR Ser. Mat.*, 15(4):309–360, 1951.

[14] Scott R. J. Report on waves. *Rep. 14th Meeting of the British Assoc. for the Advancement of Science*, pages 311–390, 1844.

[15] N. J. Zabusky and M. D. Kruskal. Interaction of "solitons" in a collisionless plasma and the recurrence of initial states. *Phys. Rev. Lett.*, 15:240–243, 1965.

[16] Michael Faraday. Xvii. on a peculiar class of acoustical figures; and on certain forms assumed by groups of particles upon vibrating elastic surfaces. 121, 1831.

[17] A. V. Vasyliev, Y. M. Romanovskii, and V. G. Yahno. *Autowave processes*. Moscow: Science, 1987.

[18] B. S. Kerner and V. V. Osipov. *Autosolitons*. Moscow: Science, 1991.

[19] Y.R. Shen. *The Principles of Nonlinear Optics*. Pure & Applied Optics Series: 1-349. Wiley, 1984.

[20] P.N. Butcher and D.N. Cotter. *The Elements of Nonlinear Optics*. 1990.

[21] R. W. Boyd. Nonlinear optics. *San Diego: Academic Press*, 1992.

[22] Stéphane Randoux, Pierre Suret, and Gennady El. Inverse scattering transform analysis of rogue waves using local periodization procedure. *Scientific Reports*, 6:29238, 2016.

[23] G. A. Askaryan. Prediction of the existence of a waveguide mode with the propagation of an electromagnetic beam. *JETP*, 42:1567, 1962.

[24] S. Novikov, S. V. Manakov, L. P. Pitaevskii, and V. E. Zakharov. *Theory of solitons: the inverse scattering method*. Springer Science & Business Media, New York, 1984.

[25] M Klaus and J. K. Shaw. On the eigenvalues of zakharov-shabat system. *J. Math. Anal.*, 34(4):759–773, 2003.

[26] G. Boffetta and A. R. Osborne. Computation of the direct scattering transform for the nonlinear schroedinger equation. *Journal of computational physics*, 102(2):252–264, 1992.

[27] M. J. Ablowitz and J. Ladik. Nonlinear differential-difference equations. *Math. Phys.*, 16:598–603, 1975.

[28] M. J. Ablowitz and J. Ladik. Nonlinear differential–difference equations and fourier-analysis. *Math. Phys.*, 17:1011–1018, 1976.

[29] G.P. Agrawal. *Fiber-optic communication systems*. Number 1 in Wiley series in microwave and optical engineering. Wiley-Interscience, 2002.

[30] R. Kashyap. *Fiber Bragg Gratings*. Electronics & Electrical. Elsevier Science, 1999.

[31] O. V. Belai, L. L. Frumin, E. V. Podivilov, and D. A. Shapiro. Efficient numerical method of the fiber bragg grating synthesis. *J. Opt. Soc. Am. B*, 24(7):1451–1457, Jul 2007.

[32] G.L. Lamb. *Elements of Soliton Theory*. A Wiley-Interscience publication. Wiley, 1980.

[33] Anastasiia Vasylchenkova, Jaroslaw E. Prilepsky, and Sergei K. Turitsyn. Contour integrals for numerical computation of discrete eigenvalues in the zakharov–shabat problem. *Optics Lett.*, 43(15):3690–3693, 2018.

[34] L. M. Delves and J. N. Lyness. A numerical method for locating the zeros of an analytic function. *Math. Comp.*, 21:543–560, 1967.

[35] Vera N. Kublanovskaya. On some algorithms for the solution of the complete eigenvalue problem. *USSR Computational Mathematics and Mathematical Physics*, 1(3):637–657, 1963.

[36] J.G.F. Francis. The qr transformation, i. *The Computer Journal*, pages 265–271, 1961.

[37] J.G.F. Francis. The qr transformation, ii. *The Computer Journal*, pages 332–345, 1962.

[38] Rene Schmogrow, Bernd Nebendahl, Marcus Winter, Arne Josten, David Hillerkuss, Swen Koenig, Joachim Meyer, Michael Dreschmann, Michael Huebner, Christian Koos, Juergen Becker, Wolfgang Freude, and Juerg Leuthold. Error vector magnitude as a performance measure for advanced modulation formats. *IEEE Photonics Technology Letters*, 24(1):61–63, 2012.

[39] J. Skaar and O.H. Waagaard. Design and characterization of finite length fibre gratings. *IEEE Journal of Quantum Eletronics*, 39(10):1238–1245, 2003.

[40] Dmitry Churkin, Srikanth Sugavanam, Nikita Tarasov, Serge Khorev, Sergey V. Smirnov, Sergey M. Kobtsev, and Sergei K. Turitsyn. Stochasticity, periodicity and coherent structures in partially mode-locked fibre lasers. 2014.

[41] G. Weerasekara and et al. Soliton's eigenvalue based analysis on the generation mechanism of rogue wave phenomenon in optical fibres exhibiting weak third order dispersion. *Opt. Express*, 23:143–153, 2015.

[42] A. Osborne. *Nonlinear Ocean Waves and the Inverse Scattering Transform*. International Geophysics. Elsevier Science, 2010.

[43] K. P. Bube and R. Burridge. The one-dimensional inverse problem of reflection seismology. *SIAM Review*, 25(4):497–559, 1983.

[44] A. K. M. Sarwar and et. al. Modified gelfand - levitan inverse scattering technique in exploration seismology: A suggestion for a fast approximate algorithm. *SEG Technical Program Expanded Abstracts*, pages 447–449, 1987.

[45] Egor V. Sedov, Alexey A. Redyuk, Mikhail P. Fedoruk, Andrey A. Gelash, Leonid L. Frumin, and Sergey K. Turitsyn. Soliton content in the standard optical ofdm signal. *Opt. Lett.*, 43(24):5985–5988, Dec 2018.